Table

sdf

Abstract

Stretchable electronics are of great interest to the industry, for the fact that it brings in flexibility compared to the tradition electronics, and this potential can significantly enlarge the application aspects.

Being one of the most widely studied stretchable electronics, gold on PDMS has its remarkable **advantages**. However, during the deposition of metal upon elastomer, unwanted cracks are commonly seen, especially under strain. We want to understand the crack evolution history corresponding to strain history, thus we want to induce the bulge test method, as a parallel experimental method to uniaxial tensile test.

To start with, we model the linear elastic behavior under bulge test, taking into account all the parameters in traditional bulge equation. Bulge test is performed on thin film by applying pressure on one side and measuring the deflection of the membrane. Mechanical properties are obtained from the pressure deflection relationship according to bulge equations. However, traditional bulge equation has its own limitation: it is more restricted to elastic materials, while the stretchable material we use, PDMS, is elastomer instead.

To overcome this limitation, we develop the bulge equation, in which the constitutive behavior of the material is also considered. Instead of merely an elastic pressure deflection relation, we obtain a hyper elastic relation, which better meets our purpose.

We then design and manufacture the device to perform bulge test. After serial of improvements, a satisfactory device ready to perform tests is produced. The manufacturing details are described.

In-situ profilometry test provides bulged membrane profiles, and thus deflection height, corresponding to specific applied pressure specific bulge device window. It gives phenomenal pressure deflection curves. By fitting them to the linear elastic and non linear hyper elastic modeling, **one can tell…** Strain history is thus controllable, according to the modelling and profilometry test, by varying pressure or window size.

In-situ optical microscope combined with bulge test can give sequence of images of crack opening under controlled increasing pressure. Pressure is related to strain through deflection, thus pressure loading history can be converted into strain history. Crack evolution is studied by manually measuring the crack displacement. A strain-displacement curve is obtained.

Up to this point, our purpose of studying relation between crack evolution and strain history is achieved, but the bulge test device can still be modified to be used in other measurement of mechanical properties of thin films. Also, a more sensitive, automative way to quantify crack evolution corresponding to strain history can be developed in the future.

1 Introduction

1.1 Stretchable electronics

Though the main tendency of study in electronics area is still to make it faster and smaller as rigid planer circuits, one cannot neglect the limitation of existing stiff structure. Stretchable electronics, on the other hand, induce more flexibility on application and thus it is becoming a new trend of research. It has significant prospective application, especially in the biomedical field, for example, skin-like sensors, flexible health monitors, wearable communication devices, and other application that require lightweight, deformable format. [1]

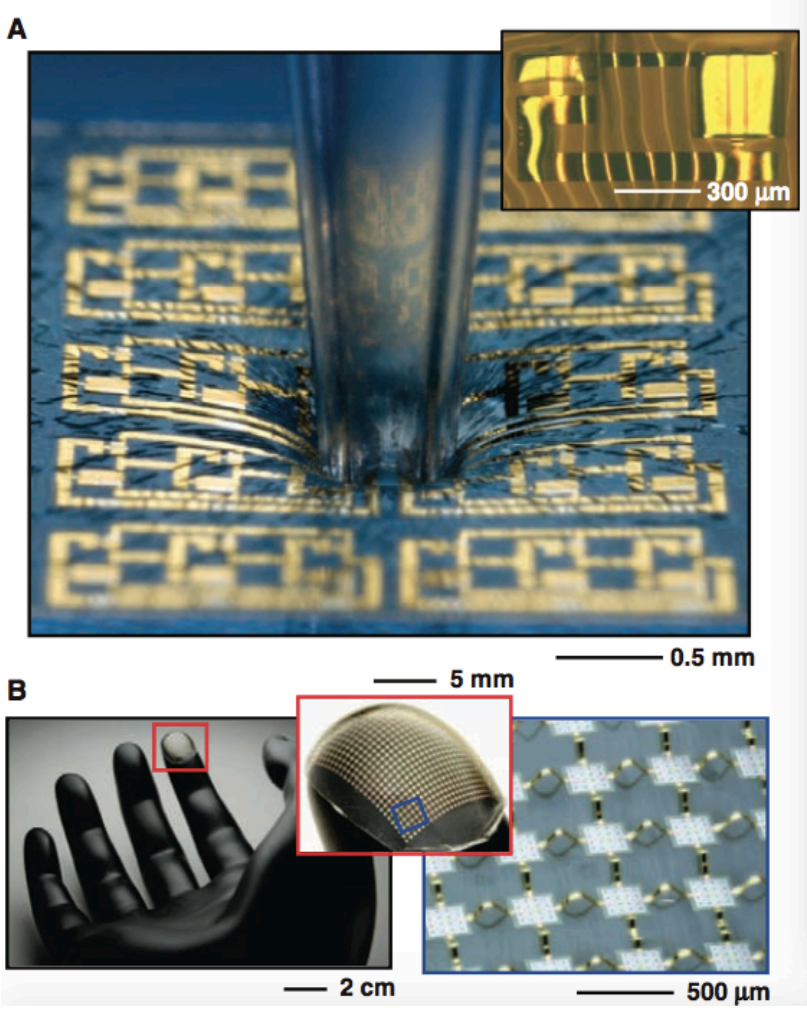

Fig. 1.1. Examples of stretchable electronics. (A) Stretchable silicon circuit in a wavy geometry, compressed in its center by a glass capillary tube (main) and wavy logic gate built with two transistors (top right inset). (B) Stretchable silicon circuit with a mesh design, wrapped onto a model of a fingertip, shown at low (left), moderate (center) and high (right) magnification. The red (left) and blue (center) boxes indicate the regions of magnified views in the center and right, respectively. The image on the right was collected with an automated camera system that combines images at different focal depths to achieve a large depth of field.

The early study of this unconventional form [2] began with polymer transistors formed on bendable plastic sheets around 20 years ago. A lot of profound success followed, with contribution of advance printing and patterning techniques, devices with hundreds of active components are nearing commercial reality. [3,4] The deepened technology involves the development of new electronic materials that can flex, such as organic semiconductors or films of carbon nanotubes [5,6], and new material conductors that can stretch, such as composite elastomer. [7,8] Two important parameters of the structure are well-studied in order to construct a stretchable structure, i.e. thickness and configuration. [9]

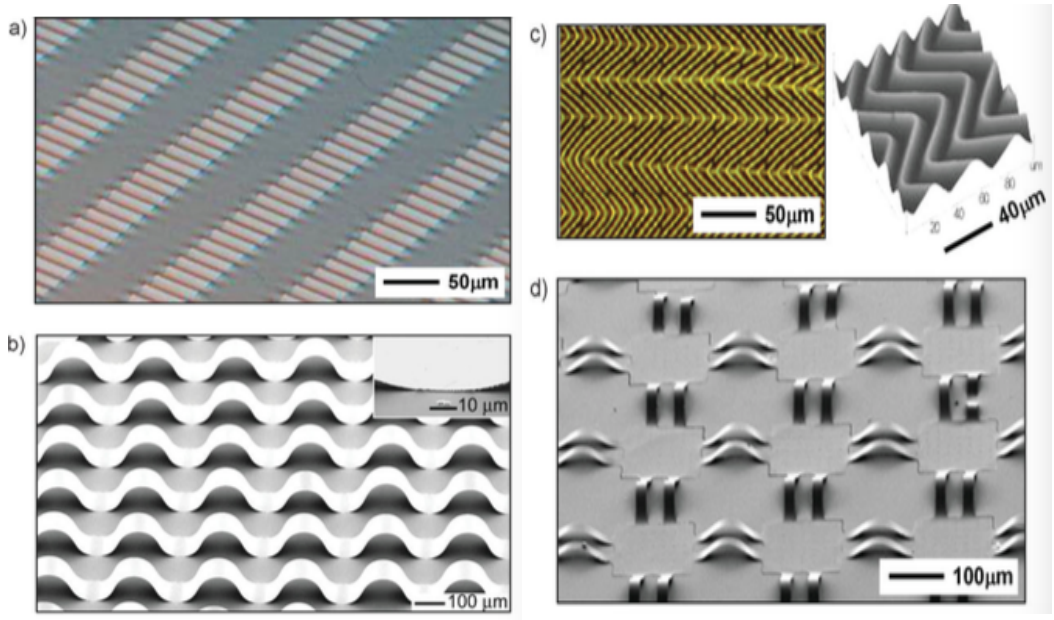

Figure 1.2. Scanning electron microscopy (SEM) and optical microscopy images of inorganic structures in controlled buckling geometries on elastomeric substrates. a) SEM image of an array of silicon nanoribbons in wavy configurations on PDMS. b) SEM image of an array of gallium arsenide nanoribbons in buckled shapes where bonding to the PDMS substrate occurs only at the positions of the troughs. c) Optical microscopy (left) and atomic force microscopy images (right) of a wavy, silicon nanomembrane bonded to a PDMS substrate. d) SEM image of a silicon nanomembrane in a buckled, mesh layout on PDMS. Bonding is localized to the regions of the square islands.

Any material in sufficiently thin form is flexible, by the virtue that bending strains decline linearly along with thickness. This mechanics stays true for even the brittle and rigid material. For example, a silicon wafer is known as brittle and rigid, but once it is fabricated in a nanoscale form, i.e. nanoscale ribbons, wires or membranes, it becomes flexible. A group of researcher has successfully achieved only 0.0005% peak strains to radii of curvature of 1cm, by making silicon as ribbons with thicknesses of 100nm. [10] This peak strain is far below the fracture limits of silicon (~1%).

Performance can be further improved by constructing such structures in stretchable configurations. Commonly used stretchable configurations are: One dimensional 'wavy' ribbon mounted to an elastomeric substrate, one dimensional buckled ribbon bonded to substrate only at positions of the troughs, two dimensional 'wavy' membrane, two dimensional buckled mesh. Examples are shown in Fig.1.2.

Other strategies, which do not involve out-of-plane motion, are also considered to be reasonable to construct stretchable inorganic structures. Coiled-spring is the first to be introduced. It obtains certain degree of stretchability if the coiled spirals are uncurled. Another planar strategy is to use leaf-arm springs. Stretchability is realized by pivoting motion mode. S-shaped (i.e., serpentine) structures are also exploited, in which bending at the corners accommodate applied strain. Examples are illustrated in Fig.1.3

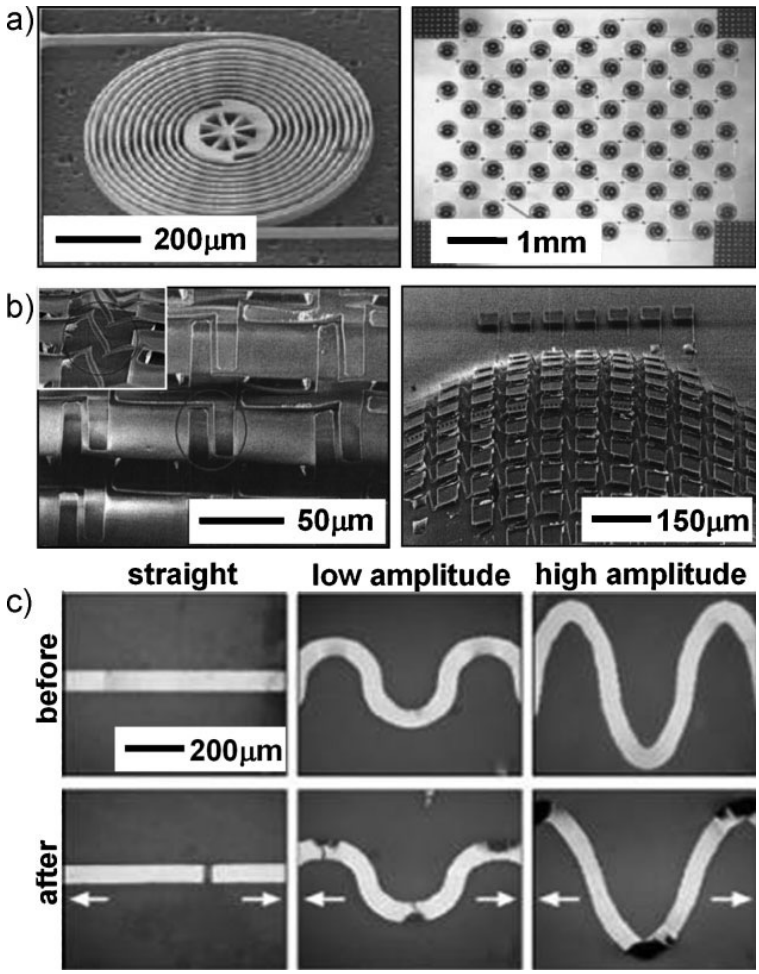

Figure 1.3. a) SEM image of an silicon structure etched into the shape of a spiral surrounding a central hub (left) and optical image of expanded, interconnected array of such structures (right). b) SEM image of silicon island interconnected with straight, leaf-spring type interconnects on an elastomeric film before (right) and after (right inset) stretching, and view of the array after expansion into a dome shape by applying pressure from the back side. c) Optical images of straight and serpentine metal lines (low- and high-amplitude structures) on an elastomeric substrate. The sequence of images on top shows the as-fabricated structures. The sequence of images on the bottom shows the same structures after application of tensile strain in the direction indicated by the arrows. The discolored regions correspond to deformations at locations of peak strain.

1.2 Material choice for stretchable electronics

Stretchable electronics require integration of microelectronics onto flexible substrates. This involves material choice for both the flexible substrate and the patterned metal layer on top.

1.2.1 PDMS as Substrate

For the sake of flexibility, most of the substrate materials chosen by researchers are polymers. The mostly used ones are: Polydimethylsiloxane (PDMS), Polyimide (PI) and polyethylene terephthalate (PET).

PDMS is chosen to be the stretchable substrate in our project. PDMS is a silicone elastomer with desirable properties and for the potential stretchable electronics application, for example, biomedical conditions. In chemical and biomedical aspects, PDMS is inert and non toxic, stable under wide temperature range, easy to prepare, handle and modify [11]. Also, PDMS is compatible with microelectronic clean room equipment after proper preparation. These features allow applications under environment as complex as inner human body, and feasibility under microfabrication using chemicals. In aspect of mechanics, PDMS with proper fabrication shows isotropic and homogeneous properties, which are important to accommodating exceeding strain from conductive layer on top. Economically, it costs much lower than silicon.

Several characterization experimental results obtained by a group of researcher (Mata et al. [11]) on five most possible used PDMS sample preparations. According to the result, chemical immersion does not show major changes in PDMS surface hydrophilicity, which indicates compatibility under microfabrication. Sterilization does not affect PDMS surface micro-textures, element concentration or hydrophilicity which proves feasibility of PDMS in

biomedical application. Immersion in tissue culture media induced an increase O/Si ratio, which may require for additional care in some specific biomedical application.

1.2.2 Gold on PDMS

Gold is one of the most ductile metal with high electrical conductivity, and also biocompatible, which meets our target to obtain stretchable electronics.

Researches have shown that gold films on PDMS membranes can be stretched far beyond strain limit of gold film alone, while still remain electrically conducting. Their stretchability can be further improved by manipulating the structure of gold films, i.e., buckles' direction, amplitude and wave length [12,13]. The reason for the increase performance is that the electrical failure of a thin metal film is mainly due to mechanical fracture, and if the film is strongly bonded to a substrate compliant enough, the failure is suppressed or delayed [12].

According to the study of stretchability of thin metal films on elastomer substrate [14], as a freestanding thin film, gold film rupture at around 1% strain. The value is smaller than that of corresponding bulk metals. The reason for this may be the fact that although a gold thin film is inherently ductile, the deformation is very localized and the film does not harden beyond modest strain. For a freestanding metal film, rupture is induced by a single neck. Once a neck is formed, further deformation of the film will take place only around this region. The film is thin, thus shows a small thickness-to-length ratio, which indicates that elongation at the single neck contributes very little to the overall rupture strain. This group of researcher proved that with larger rupture strains can be achieved by bonding the metal film to an elastomer substrate well and firm. Lacour et al. [15] attempted and succeeded in obtaining additional stretchability of a few tenths of a percent by inducing a surface wave, i.e. random wrinkles, in thin gold film.

There are other researches on improving stretchability of thin gold film on PDMS substrate, which indicates a promising reliability to start with this

specific configuration. Although gold is not economically low cost, the advantage of its ductility, conductivity and biocompatibility trigger the interest of ours.

1.3 Alternative testing methods for thin film properties

Alternative to bulge test method, which is the testing method we process and perform in this project, there exist several other testing methods to obtain thin film properties. The most significant two are uniaxial tensile test and nanoindentation. For the sake of completeness, both techniques are listed as introduction.

1.3.1 Uniaxial micro tensile test

Uniaxial tensile test can measure strain directly on the specimen with suitable extensometers. But for thin films with refined thickness, this technique requires special techniques and procedures for sample preparation, handling and loading. Comparing to the traditional uniaxial tensile test in marco scale, the alignment and gripping system should be specially taken care of, for the fact that a trivial error in performance will induce large deviation in the micro scale experiment.

Two different kind of set up will be introduced in this section, both of which are mostly referred to by the latter researcher. The first one of was built up by Sharpe et al. [15], the second was by Ogawa et al. [16].

1) Sharpe et al. [15]

   In this system, strain is measured with the interferometric strain/displacement gage (ISDG). Precise load measurement is enabled by am air bearing system to avoid friction and a periodically calibration is done to loading system. Both strain and load are measured and recorded to a computer on a real-time basis.

   The ISDG is an optical technique to measure strain or displacement between two reflective gage markers on the specimen. Young's two-slit

interference served as optical principle of ISDG, but reflection is detected instead of transmission.

A pair of gold pads or lines are deposited on the specimen as marker to generate interference fringe from their slightly inclined edges.

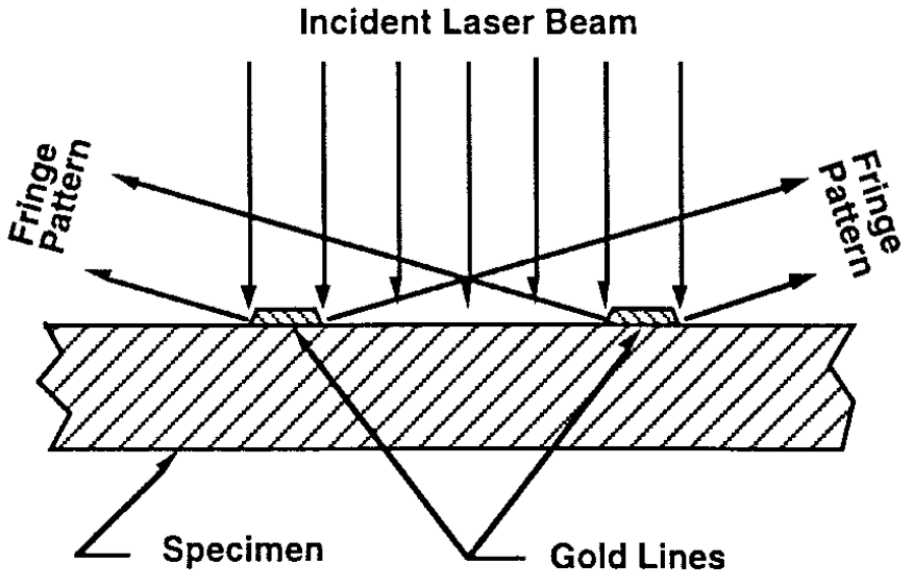

Figure 1.4. Schematics of the ISDG

When both markers are illuminated with laser, a diffracted reflection interfere with each other, so the fringes are formed. While markers move relative to each other, the fringe patterns change and the motion can be detected so as to obtain relative displacement due to strain. Rigid-body motion will also cause the fringes to move, so it is necessary to average the movement of the two fringe patterns. The equation to obtain strain from fringe motion is :

$$\varepsilon = \frac{\lambda}{2d_0}\left(\frac{\Delta m_1}{\sin\alpha_1} + \frac{\Delta m_2}{\sin\alpha_2}\right)$$

Here Δm_1 and Δm_2 are the relative fringe shifts of patterns, d_0 is the intial gage length between the indentations, λ is the wavelength of the

laser, and α_1, α_2 are the angles between the incident laser beam and fringe patterns.

The fringe patterns can be converted into electrical signals with diode. Relative uncertainty of this kind of test are around $\pm 3\%$, with contribution from original gage length measurement, locating minimum and angle measurement.

Specimens used in this uniaxial micro tensile test should be manufactured and handled uniquely. Fig 1.5. shows the specimen schematic. Noted that support strip is defined at top and bottom, and a rectangular area in the center is etched away so to free the specimen between two grip ends.

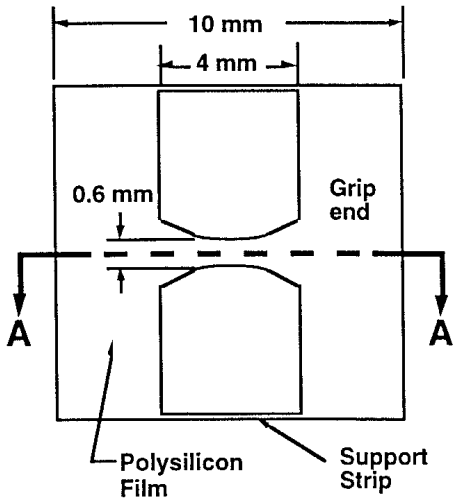

Figure 1.5. Schematics of a manufactured specimen

Fig 1.6 shows a possible release handling of specimen process.

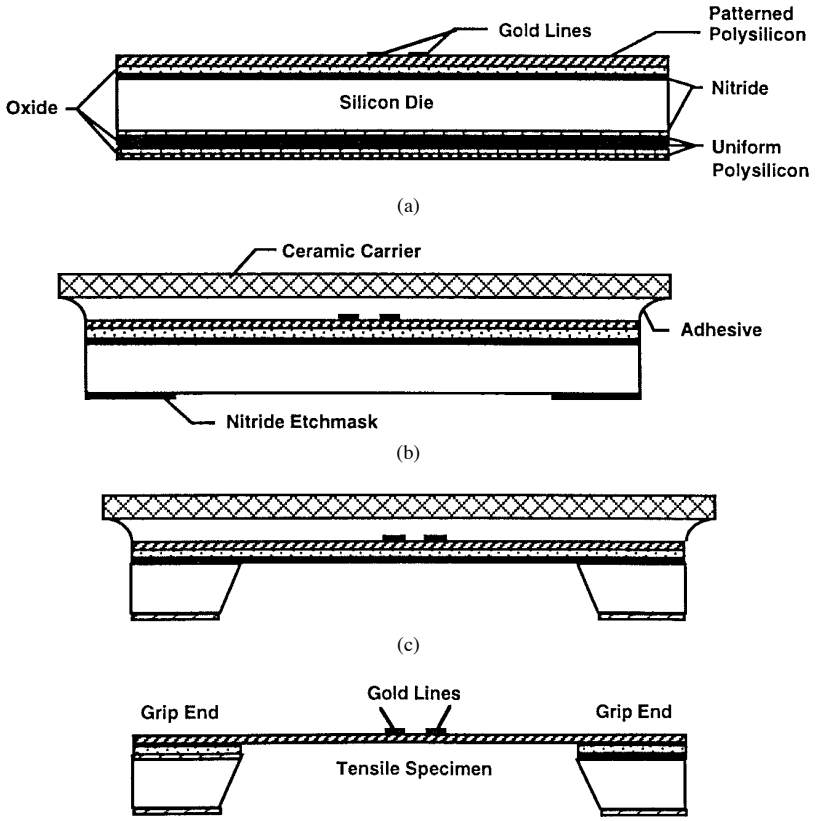

Figure 1.6. Steps to release the tensile specimen viewed in section A-A

A ceramic carrier is mounted on the die using adhesive wax, which aims to protect the polysilicon specimen.

A schematic of the measurement system without the microcomputer, which control tests and records data. The grip is fixed on one side and attached to a linear air bearing on the other. The linear air bearing, which is used to minimize the friction in loading system so as to gain accurate load measurement, connects to a load cell. Displacement or load is applied by the piezoelectric actuator which follows commands from computer, thus load is recorded simultaneously. The fringe motions are converted into strain. Combining two, we obtain the load-strain curve.

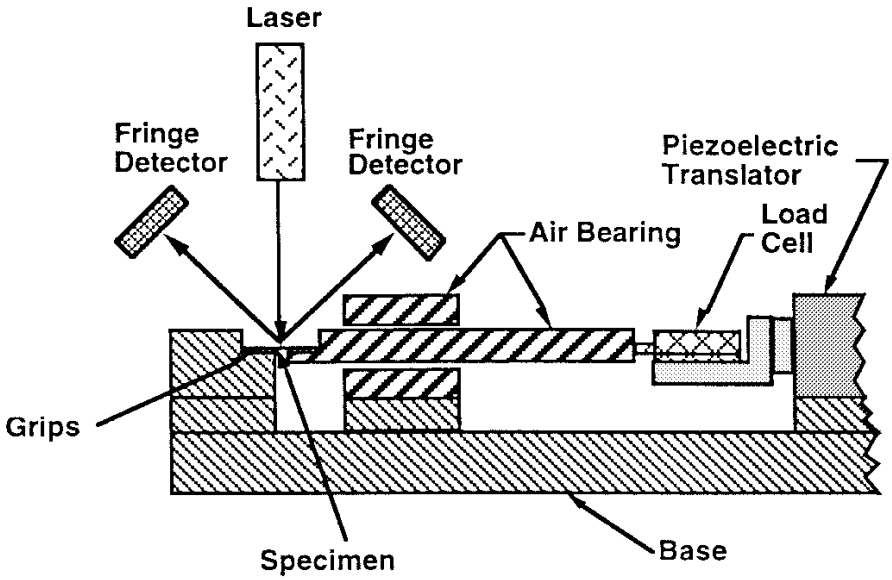

Figure 1.7. Schematic of the measurement system

2) Ogawa et al. [16]

The uniaxial tensile test set up by Ogawa et al. differs from the one done by Sharpe et al., but not significantly. Following the similar procedure, marked specimens with identical shape are obtained.

The strain was determined by measuring the relative displacement of the marks, but instead of using laser interferometer, a double-filed-of-view microscope is used, combining with two CCD cameras and image

synthesizer and an image processor. That is to say, strain is measured by processing the images.

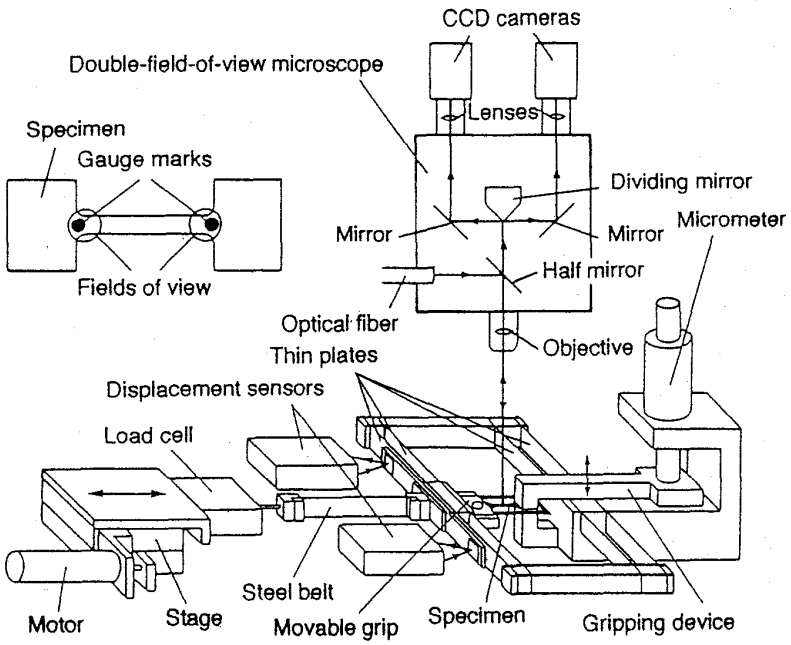

Figure 1.8. Schematic of the tensile test machine set up

To mount the specimen on the machine and grip it, the group of researchers design a different mechanism. The specimen is mounted on the movable grip and clamped with a screw and a plate, then it is better fixed by a micrometer.

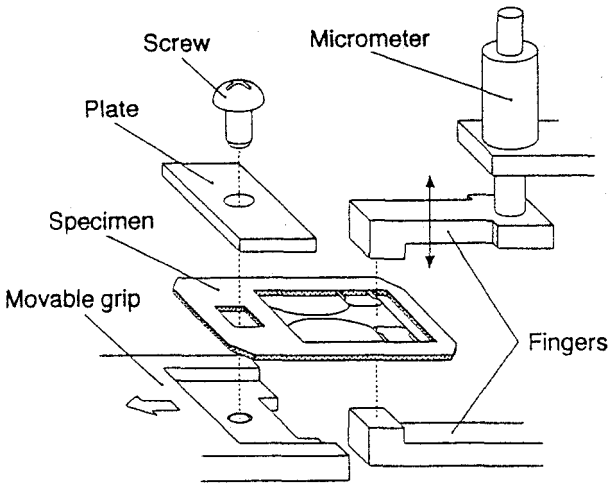

Figure 1.9. Schematic of the specimen mounting

1.3.2 Nanoindentation [17] [18]

Nanoindentation is one of the most widely used test method to study mechanical properties of thin films. A sharp diamond is indented into the surface of the specimen thin film on a substrate, force imposed and corresponding displacement of the indenter are both measured.

Nanoindentation technique can measure hardness, elastic properties and time-dependent deformation of thin films. It can also serve as an indenter to induce fracture of sub-micron scale, for the measurement of fracture toughness. Fig.1.x shows the most commonly used tips and their indentation shape for nanoindentation techniques.

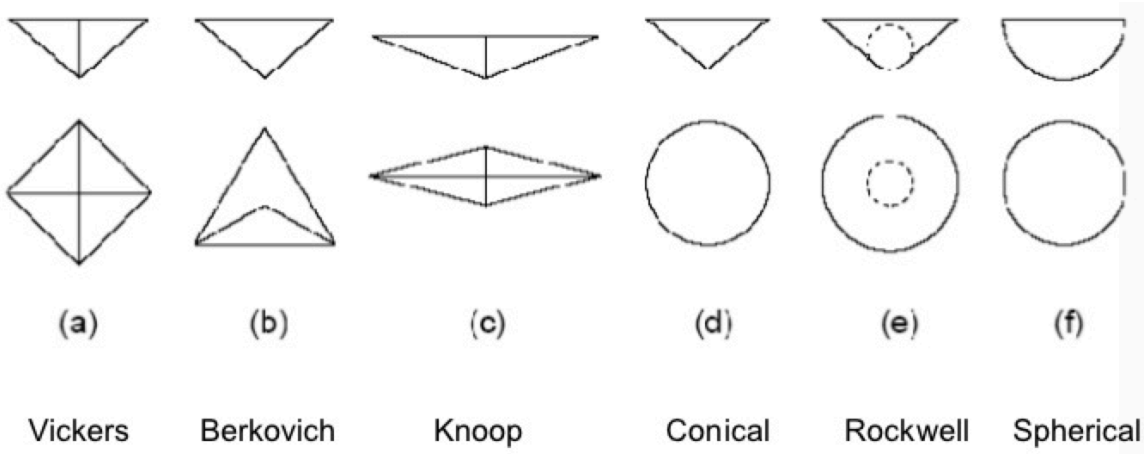

Figure 1.10. Schematics of most commonly used tips and corresponding indentation shape

In the nanoindentation test, indentation load is controlled and indenter displacement is measured. A known stiffness indenter (mostly diamond) with calibrated shape is pressed into the sample, the sample surface deforms both elastically and plastically, a conforming shape hardness impression is formed. While the indenter withdraws, only the elastic portion of deformation is recovered. Hence a load-displacement curve can be obtained and desired properties can be abstracted and calculated through the curve.

Several new instruments combined with an AFM system which enable nanoindentation techniques to not only record load and depth of indentation, but also images before, during and after process. This provides useful qualitative information about test, but it is not sufficiently accurate to measure directly the contact area, which is used in calculating hardness and elastic modulus.

Fig.1.x. shows a schematic diagram of the Nanoindenter. The load is applied and controlled by the current in the coil coupled with a permanent magnet. Indenter column is supported by a very delicate leaf springs, which are part of the capacitance device for measuring displacement.

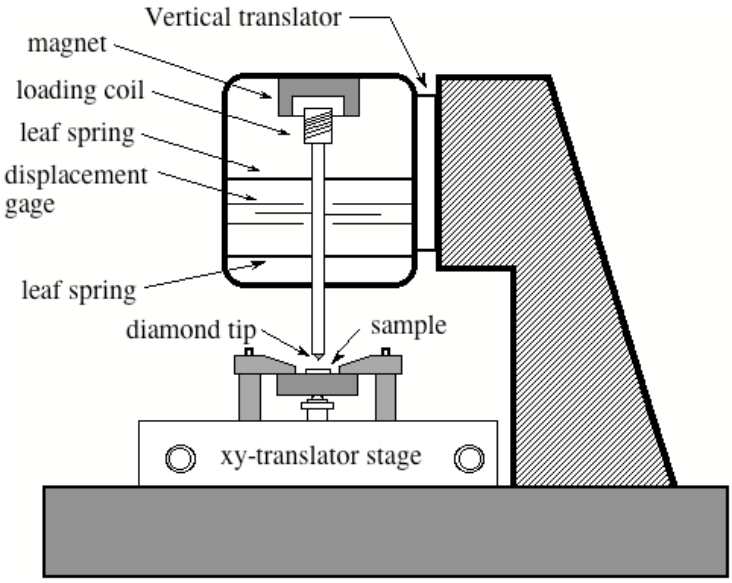

Figure 1.11. Schematics of most commonly used tips and corresponding indentation shape

Hardness is defined as the indentation load divided by projected contact area of indentation.

$$H = P_{max}/A.$$

Measurement of the projected contact area A from a load-displacement curve requires h_c, the contact depth. For an indenter with a known geometry, for example, an ideal Berkovich indenter,

$A = 24.56h_c^2$

Further calibration is needed, if the Berkovich indenter is not perfecty sharp, calibration constants can be obtained by fitting p-d curves of several attempts. The contact depth can be estimated from the load-displacement data:

$$h_c = h_{max} - \varepsilon \frac{P_{max}}{S}$$

Here ε is a constant that depends on the indenter geometry, for Berkovich it is 0.75.

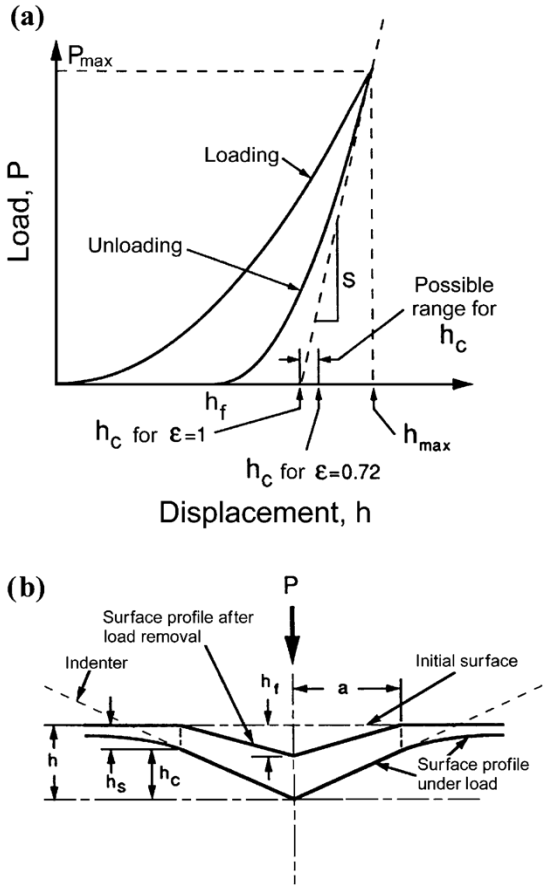

Figure 1.12. (a) A typical load-displacement curve; (b) the deformation pattern of an elastic-plastic sample during and after indentation.

The elastic modulus of the indented sample can be obtained by the initial unloading contact stiffness, i.e., the slope of the beginning part of the unloading curve.

$$S = dP/d\mathrm{h}$$

$$S = 2\beta\sqrt{\frac{A}{\pi}}E_r$$

$$E_r = \frac{1-\nu^2}{E} + \frac{1-{\nu_i}^2}{E_i}$$

Here β is a constant that depends on geometry of indenter, for Berkovich it is 1.034, and E_r is the reduced elastic modulus, due to the fact that both the sample and the indenter deform. E and ν are the elastic modulus and Poisson's ratio for the sample, while E_i and ν_i are those of indenter. $E_i = 1141\ GPa$ and $\nu_i = 0.07$, for diamond.

It should be noted that the elastic properties from previous equation hold for the sample thin film only when the film thickness is much greater than the indentation depth. Otherwise the properties obtained are those of the substrate.

In this section, two testing method for thin films, which are alternative to bulge test, are introduced. They both have their limitations. For uniaxial micro tensile test, the experimental result suffers from alignment and gripping of the setup, while for nanoindentation, the result would be affected by the presence of substrate. Thus, bulge test is induced in the group of techniques to measure thin film properties. And it is the one that we try to build up and develop in our project.

2 Theoretical Principles [17]

This chapter is about the bulge test method used in this project. After brief history of this specific technique, the theory of bulge test will be presented. Bulge equations for different window shape will be delivered. Later, the general setup for bulge test will be describe, as guidance to the manufacture and mounting in our project.

2.1 Bulge test introduction

Thin films have important applications as mentioned before. But to take full advantage of these materials and to improve reliability, one should understand well the mechanical behavior of thin films.

The mechanical properties of thin films and the residual stresses in them are recognized to be crucial in the fabrication of electronic devices and sensors in microscale shape and size. This gives motivation for research of mechanical properties of thin films. But the techniques commonly used in bulk material measurements cannot be directly applied to thin films. Thus during decades researchers devoted to setup suitable testing methods to be used.

There are several specialized techniques for measuring the mechanical properties of thin films, as introduced before. However, the information that can be obtained from these techniques is somehow limited. For example, nanoindentation is often affected by the substrate, and the micro-tensile test suffers from difficult sample handling as well as the alignment and gripping problems [26]. Bulge test has its unique advantages of precise sample fabrication and minimal sample handling. It is a non-destructive test method (compared to nanoindentation), and gives result of biaxial properties, Poission ratio and initial stress (compared to uniaxial tensile stress test).

Bulge test determines mechanical properties of free standing thin films by applying pressure on one side and measuring the corresponding deflection. Its theory was first developed in 1915 by Hencky. [19] Beams [20] then introduced this idea into measurement of material properties. He began with very simple pressure deflection relationship, which lack further theoretical backup. Later, Tsakalakos [21] developed the theory for circular membranes. Small [22] took into consideration also the intrinsic stress of the film and initial height of the membrane. Vlassak and Pratt [23],[24] developed the theory for square membrane, but it is still too complex and thus lack of further usage. Likewise, Tabata and Vlassak [25],[23] developed the theory for rectangular membranes, and this improvement supports a broadened variety of application.

2.2 Bulge equations

Bulge test determines mechanical properties of free standing thin films by applying pressure on one side and measuring the corresponding deflection.

The central deflection (*h*) is directly related to the strain in the window while applied pressure (p) is related to stress. Thus, mechanical properties of thin film material can be extracted from knowing the window size, and measurement of pressure and deflection.

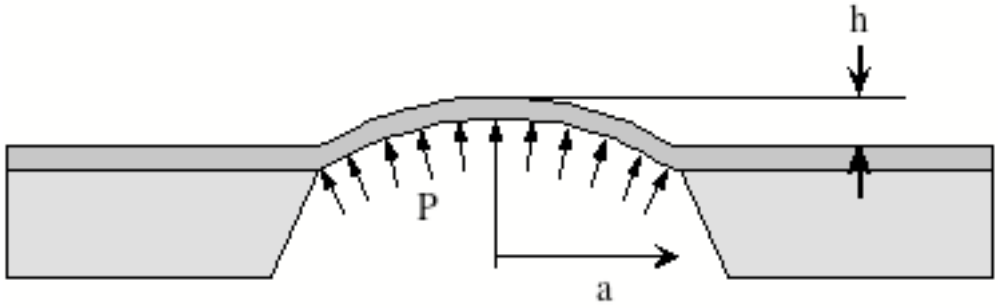

Fig.2.1. Main parameters in bulge test method

Bulge test has different models corresponding to different window shape. The table below shows summary of different geometries used for bulge test. Later in this chapter, the path to obtain bulge equations will be illustrated.

Table 2.1. Summary of the different geometries used for bulge test

Geometry	Stress/Strain state of the center of the membrane	Stress and Strain	Bulge Equation $p = C_1\sigma_0 t\frac{\delta}{a^2} + C_2\frac{E}{1-\nu}t\frac{\delta^3}{a^4}$
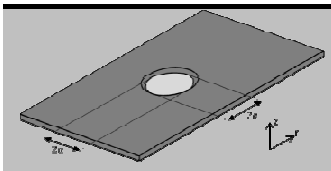	Equi-biaxial stress $\sigma_{tan} = B(\varepsilon_{tan} - \varepsilon_0) + \sigma_0$	$\sigma_{tan} = \frac{a^2 p}{4\delta t}$ $\varepsilon_{tan} = \frac{2\delta^2}{3a^2} + \varepsilon_0$	$C_1 = 4$ $C_2 = \frac{8}{3}$
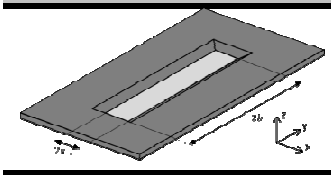	Plane strain $\sigma_{tan} = M(\varepsilon_{tan} - \varepsilon_0) + \sigma_0$	$\sigma_{tan} = \frac{a^2 p}{2\delta t}$ $\varepsilon_{tan} = \frac{2\delta^2}{3a^2} + \varepsilon_0$	$C_1 = 2$ $C_2 = \frac{4}{3(1+\nu)}$
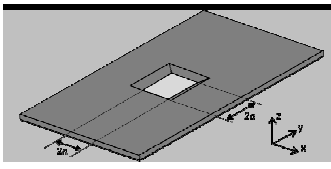	Transition state	No straight forward analytical expression	$C_1 = 3.939$ $C_2 = \frac{1}{(0.792 + 0.085\nu)^3}$

2.3 Spherical window model of the bulge test

A pressurized thin-film clapped by circular window can be modeled as a section of a thin-walled spherical cap.

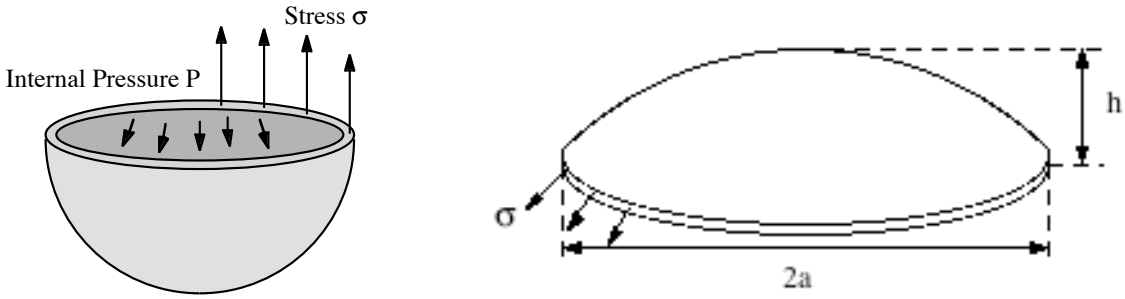

Fig.2.2. Schematic sketch of a bulged film in spherical shape

Wall thickness is t, and radius is R (not indicated in the picture). The stress in the thin wall is obtained by force equilibrium due to stress and pressure.

$$p \cdot \pi R^2 = \sigma \cdot 2\pi R t$$

$$\sigma = \frac{pR}{2t}$$

Noted that $2\pi Rt$ is actually the cross section area of thin wall. Here, in the spherical bulge model, the stress is in-plane and equi-biaxial, ($\sigma_{xx} = \sigma_{yy}$). We also call it as plane stress condition. These equations indicate the relationship between applied pressure, radius of curvature, and stress in the bulged thin film.

A bulged film in reality (right of Fig.3.3) is like a slice of the spherical vessel on the left. Letter “a” indicates window radius. As mentioned in the title, the window is manufactured in spherical shape.

In general bulge test models, one considers only relatively small deflections ($h \ll a$). From pure geometry, one can write the relationship between deflection height, window size and membrane curvature radius.

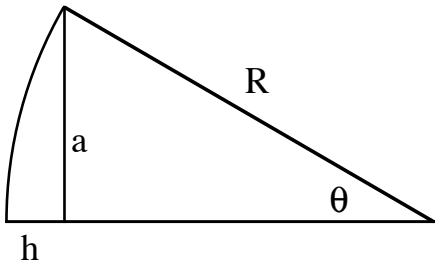

Fig.2.3. Schematic sketch of cross section of thin film and its geometry

The relation can be written as:

$$R^2 = (R-h)^2 + a^2 = R^2 - 2Rh + h^2 + a^2 \approx R^2 - 2Rh + a^2$$

Noted that h^2 is relatively small, as mentioned before, thus h^2 is neglected. So we can rearrange the equation and get:

$$R = \frac{a^2}{2h}$$

By making a substitution to the previous expression, one can get the stress expression:

$$\sigma = \frac{pR}{2t} = \frac{pa^2}{4th}$$

Then we can consider about strain, to correlate to material properties. The relationship between deflection and film strain can be obtained by pure geometry:

$$\varepsilon = \frac{R\theta - a}{a} = \frac{\theta - (\frac{a}{R})}{(\frac{a}{R})}$$

Using Taylor Expansion, one can get:

$$\theta = arcsi\,n\left(\frac{a}{R}\right) = \left(\frac{a}{R}\right) + \frac{\left(\frac{a}{R}\right)^3}{6} + \cdots$$

We reserve the first two terms and strain can be expressed as:

$$\varepsilon = \frac{a^2}{6R^2} = \frac{2h^2}{3a^2}$$

For linear biaxial elastic strain,

$$\sigma = B\varepsilon = \frac{2Bh^2}{3a^2}$$

Where $B = E/(1-\nu)$ is the reduced modulus in equi-biaxial conditions.

Recalling the relationship of stress and pressure, and we get:

$$\sigma = \frac{pa^2}{4th} = \frac{2Bh^2}{3a^2}$$

By rearranging the equation, we can get the desired deflection-pressure relationship:

$$\boldsymbol{p = \frac{8Bth^3}{3a^4} = \frac{8}{3}\frac{h^3}{a^4}\frac{Et}{1-\nu}}$$

This is the bulge equation for spherical window.

If we consider also the residual stress of the membrane, we can simply rewrite the stress strain relationship, including also residual stress in material behavior.

$$\sigma = B\varepsilon + \sigma_0 = \frac{B2h^2}{3a^2} + \sigma_0 = \frac{pa^2}{4th}$$

So the bulge equation becomes:

$$p = \frac{8Bt}{3a^4}h^3 + \frac{4\sigma_0 th}{a^2}$$

But in our project, residual stress is not considered at the moment. It is just presented here as a theoretical backup, and it maybe useful for the future exploit of bulge test.

2.4 Rectangular window model for bulge test

Rectangular window is in fact the mostly used shape for bulge test device, due to its easier control over shape. Rectangular constrain also induce a biaxial behavior, but it is no longer equi-biaxial. Instead, in this model, the membrane is in plane-strain condition.

When one constructs a rectangular window for bulge test, the aspect ratio (b/a) should be larger than four, in order to immune from shape deviation effect [25]. By looking at the strains along a-direction and b-direction, one can tell that as long as aspect ratio is large enough (b/a> 4), strain in a-direction is relatively large, while strain in b-direction is very small and thus can be neglected. Furthermore, away from the ends of the rectangle, the film is assumed to have a uniform radius of curvature.

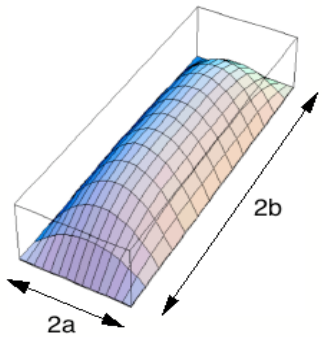

When the strain in one direction is almost zero, plane strain condition occurs. We can write the stress-strain relationships in this condition: (x is the direction of a while y is the direction of b.)

$$\varepsilon_{xx} = \frac{1}{E}\left(\sigma_{xx} - \nu\sigma_{yy}\right)$$

Fig.2.4. Schematic sketch of rectangular window shaped membrane

$$\varepsilon_{yy} = \frac{1}{E}\left(\sigma_{yy} - \nu\sigma_{xx}\right) = 0$$

So we can get that

$\sigma_{yy} = \nu\sigma_{xx}$

$\varepsilon_{xx} = \sigma_{xx}(1 - \nu^2)/E$

Like in the previous plane stress condition, we can consider $(1 - \nu^2)/E$ as the reduced modulus in the plane strain case.

In the spherical model, we consider the thin film as thin-walled spherical cap, while in the rectangular window, we can model the deformed membrane as a cylindrical thin wall.

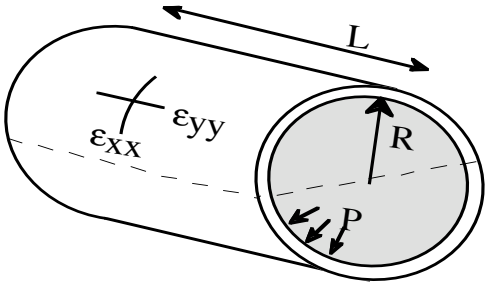

Fig.2.5. Schematic sketch of cylindrical thin-walled model

The thickness of the fall is noted as "t". So we can write again the equation due to force equilibrium. That is to say, the forces on each half of the cylinder must add to zero.

$2R \cdot L \cdot p = 2t \cdot L \cdot \sigma_{xx}$

Thus $\sigma_{xx} = Rp/t$

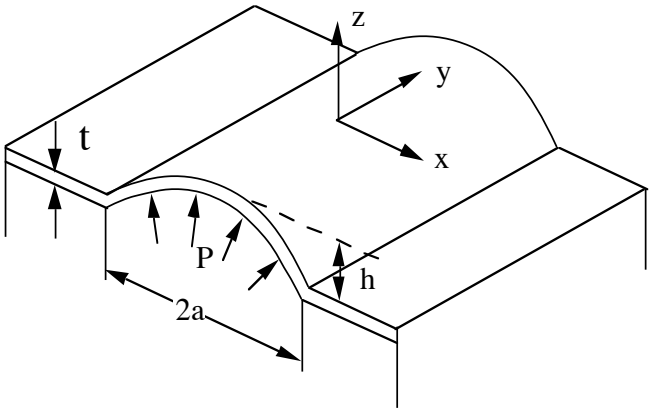

Fig.3.6. Schematic sketch of model of bulged rectangular membrane

We obtained the relationship between stress and pressure, so now we can derive a bulge equation to describe long rectangular windows.
The membrane is in plane strain condition, recall the elastic relationship we obtained from the beginning:

$$\sigma_{xx} = \varepsilon_{xx} \frac{E}{1-\nu^2}$$

And combine with the stress-pressure relationship we derive before:

$$\sigma_{xx} = \frac{Rp}{t}$$

Noted that we gained already the geometric arguments between strain, curvature, deflection and window size:

$$\varepsilon_{xx} = \frac{2h^2}{3a^2}$$

$$R = \frac{a^2}{2h}$$

So one can obtain bulge equation for rectangular membrane model:

$$\boldsymbol{p = \frac{3}{4}\frac{h^3}{a^4}\frac{Et}{1-\nu^2}}$$

If we induced also the effect of residual stress, like we did in the circular model, we can get:

$$\sigma_{xx} = \frac{2h^2}{3a^2} \cdot \frac{E}{1-\nu^2} + \sigma_0$$

$$p = \frac{2ht\sigma_0}{a^2} + \frac{4}{3}\frac{h^3}{a^4}\frac{Et}{1-\nu^2}$$

2.5 Square Windows

The last shape of window to mention about is square ones. The model is still not fully understood by now, the problem of deflection is difficult to solve analytically. Thus, it is not included in our project of realization of the bulge device. However, as a completion of theoretical knowledge, and as backup of future guidance, the square model is induced in this chapter.

In square windows, deflection is not defined to a single direction. It varies two dimensionally. Solutions are not easy to be found because of this. The approximate ones are obtained using energy-minimization method. Below the outline of procedure is listed.

1. Assume there exist a certain form of displacement function, with unknown coefficients (A, w_0, w_1) to be determined. They are equivalent to the first two terms of a Taylor series expansion. Quantities of displacements in the (x,y,z) direction are (u,v,w) respectively.

$$u = \frac{A}{a^4} x(a^2 - x^2)(a^2 - y^2)$$
$$v = \frac{A}{a^4} y(a^2 - x^2)(a^2 - y^2)$$
$$w = \frac{w_0}{a^4}(1 + \frac{w_1}{a^2}(x^2 + y^2))(a^2 - x^2)(a^2 - y^2)$$

2. Strains can be derived from the displacement functions:

$$\varepsilon_{xx} = \frac{\partial u}{\partial x} + \frac{1}{2}\left(\frac{\partial w}{\partial x}\right)^2$$
$$\varepsilon_{yy} = \frac{\partial v}{\partial y} + \frac{1}{2}\left(\frac{\partial w}{\partial y}\right)^2$$
$$\varepsilon_{xy} = \frac{\partial u}{\partial y} + \frac{\partial v}{\partial x} + \frac{\partial w}{\partial x}\frac{\partial w}{\partial y}$$

3. Energy is balanced. The total potential energy of the membrane is equal to the strain energy minus the work done by the applied pressure:

$$V = \frac{Et}{2(1-\nu^2)} \iint (\varepsilon_{xx}^2 + \varepsilon_{yy}^2 + 2\nu\varepsilon_x\varepsilon_y + \frac{1}{2}(1-\nu^2)\varepsilon_{xy})dxdy - \iint pwdxdy$$

4. Minimize the total potential energy with respect to each of the coefficients in order to solve the unknown coefficients:

$$\frac{\partial V}{\partial A} = 0, \qquad \frac{\partial V}{\partial w_0} = 0, \qquad \frac{\partial V}{\partial w_1} = 0$$

5. There are three equations and three unknowns to solve.

It is not an easy procedure, and the final result is quite similar to that obtained from the spherical cap model:

$$\boldsymbol{p = \frac{1}{(0.792 + 0.085\nu)^3} \frac{Et}{1-\nu} \frac{h^3}{a^4} + \frac{3.393\sigma_0 th}{a^2}}$$

2.6 Conclusion and discussion

Comparison and discussion of result

By comparing the bulge equation that we obtained from spherical model, rectangular model and square model, we can see the main differences are:

1) The numerical coefficients before two terms.
2) The reduced modulus is different for rectangular model.

Thus, if we can combine experiment data from rectangular windows, and either square or round windows, and neglecting the effect or residual stress, we can get two equations for two unknowns: E and ν. Thus we can obtain Young's Modulus and Poisson Ratio.

Possible sources of error in bulge test

Here listed several common cause of error within bulge test.

1) Mounting the film

   The delicate mounting would be discussed in future chapter. But one should notice that experiment condition and the proficiency of performer is one of the crucial aspect to ensure a better result. While mounting the film, one should try his best to ensure that the film is well-supported, free-standing and not wrinkled. Any wrinkling can result in significant errors.

2) Non-flat Films

The initial condition of the film is another major problem that one may face while performing a bulge test. Especially when using the laser interferometry to measure deflection, one should ensure that the film is flat within the resolution of the equipment. Otherwise, one should modify the equation by inducing an "initial height":

$$p = \frac{c_1 \sigma_0 t}{a^2}(h - h_i) + \frac{c_2 E t}{(1-\nu)a^4(h-h_i)^3}$$

3) Residual Stress

From the previous equations we can learn that residual stress take part in affecting the final accuracy of experiment. Residual stress is induced mainly during the sample preparation. It is not fully understood, and can not be predicted quantitatively easily, nor can it be avoided completely. Thus, some errors, or deviations, are to some extent foreseen.

3 Numerical modeling

As we can see in the previous chapter, by controlling pressure and window size, and measuring the deflection height, one can obtain material properties with use of bulge equation. A pressure-deflection relationship is desired to be better understood, such that by manipulating either pressure or window size, or both, we can have a known strain loading in the membrane. In this way, the strain history is controlled, and the crack evolution history of our Au/PDMS samples can be studied. We construct a numerical modeling in MATLAB in order to obtain this relationship.

A key assumption is made that the extremely thin gold layer on top does not effect PDMS membrane behavior significantly, and that residual stress is ignored at the moment. Thus in this numerical, only the PDMS properties are referred to. Meanwhile, for the lack of further deepened study on the square window cases, we did not include it in modelling nor in actual device fabrication.

In real manufacture, only the spherical windows are used. But for the sake of completeness, and for future guidance, the rectangular membranes can also be included in the modeling. It differs from the spherical model mainly by the coefficient of bulge equations and the reduced modulus.

3.1 Modeling of bulge equation in linear elasticity

The bulge equations for different window shapes in existing references are constructed under elastic conditions. Thus we start with modeling with equations, try to estimate the membrane evolution in linear elastic assumptions.

3.1.1 Strain-deflection relation

Pressure is directly related to deflection height from bulge test, thus the strain-deflection relation is of reference interest to consult corresponding strain with experimental deflection height data. Recall the equations from the previous chapter,

$$\varepsilon = \frac{R\theta - a}{a} = \frac{\theta - (\frac{a}{R})}{(\frac{a}{R})} \approx \frac{a^2}{6R^2} = \frac{2h^2}{3a^2}$$

We can have plot of strain-deflection in both spherical and rectangular window cases. According to the possible window size we may obtain from manufacture, a, in unit of μm, equals to 500, 1000, 1500, 2500 respectively.

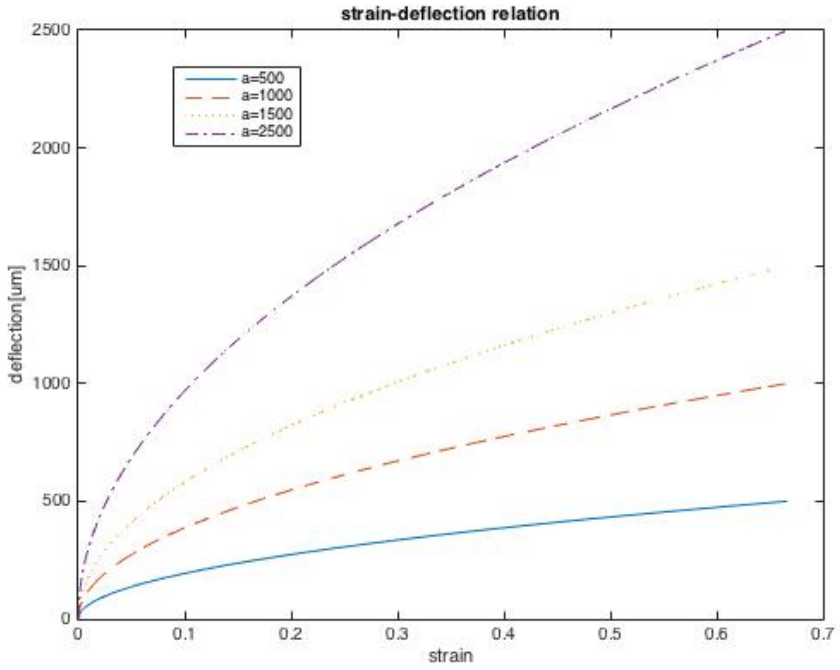

Fig.3.1 Strain-deflection relation curve

However, one should keep in mind that the strain-deflection conversion equation above is assumed to small deflection ($h<<a$). The plot is stopped at strain equals to $\pi/2$, while membrane is bulged as hemisphere. Spherical model no longer holds for further deformation and thus is not considered.

3.1.2 Linear elastic pressure-deflection relation

Recall the bulge equation from chapter 2,

$$\boldsymbol{p(spherical)} = \frac{\mathbf{8}}{\mathbf{3}}\frac{\boldsymbol{h^3}}{\boldsymbol{a^4}}\frac{\boldsymbol{Et}}{\mathbf{1-\nu}}$$

$$\boldsymbol{p(rectangular)} = \frac{\mathbf{4}}{\mathbf{3}}\frac{\boldsymbol{h^3}}{\boldsymbol{a^4}}\frac{\boldsymbol{Et}}{\mathbf{1-\nu^2}}$$

We can see that, the linear elastic pressure-deflection relationship depends on the window size, the thickness of the membrane, the elastic modulus and the Poisson ratio of the material. For the PDMS samples we are using, Young's Modulus is roughly 1Mpa, Poisson ratio is 0.5, and the thickness of the membrane is 100 μm.

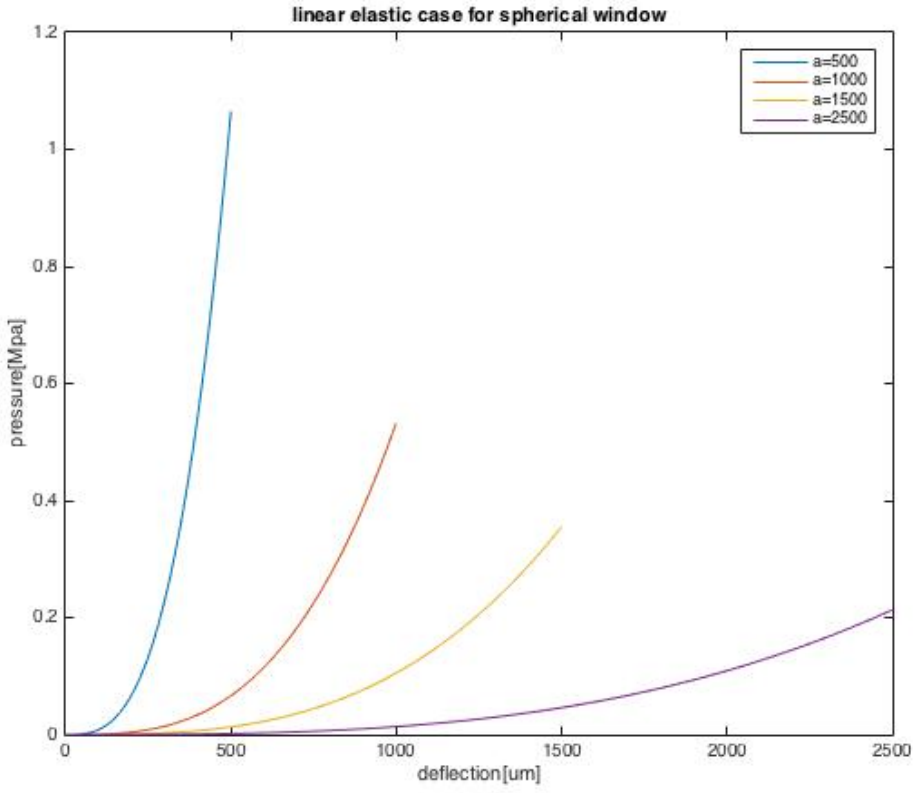

Fig.3.2. Linear elastic pressure-deflection behavior for spherical window

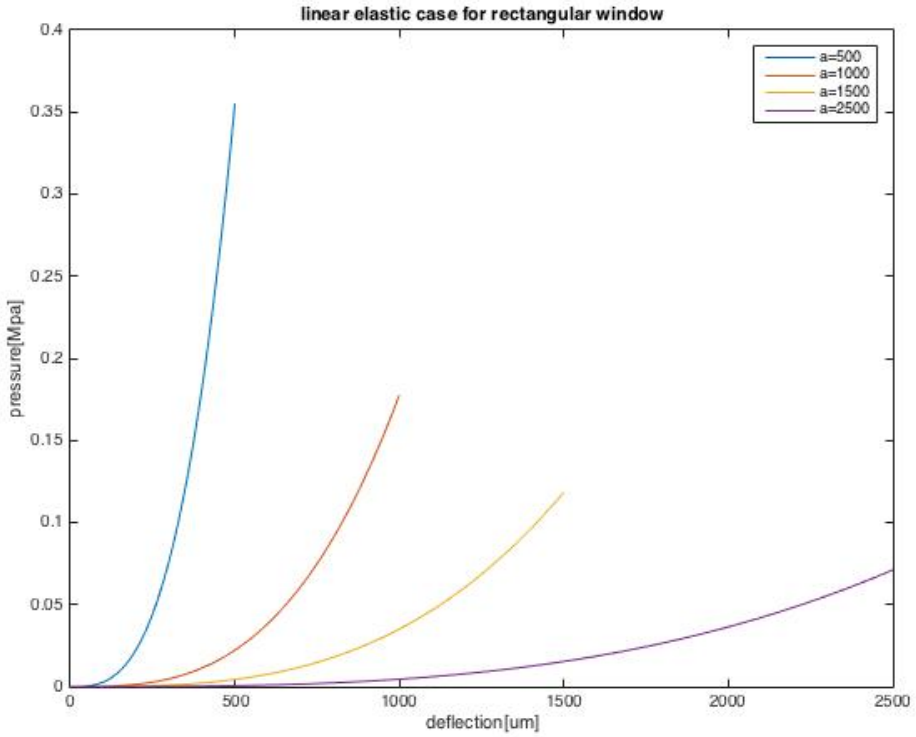

Fig.3.3. Linear elastic pressure-deflection behavior for rectangular window

Comparing the two graphs, we can see that while the tendency of curves is roughly the same (pressure is proportional to cubic of deflection height in both case), in rectangular case, the pressure to have a same deflection is much less than that in spherical case. We can derive the comparison of coefficient from the bulge equation and specific Poisson ratio for PDMS,

$$\boldsymbol{p(spherical)\sim\frac{16}{3}h^3},\ \ \boldsymbol{p(rectangular)\sim\frac{16}{9}h^3}$$

That is to say, to bulge a PDMS membrane to a certain deflection height, one should provide 3 times the pressure in the spherical window device, then that in the rectangular ones.

This result gives some experimental instruction: in some conditions, the pressure that can be built up inside the device may be limited, to gain enough deflection, thus enough strain, to conduct further observation, one can consider to use rectangular window instead of a spherical one.

3.2 Development of hyperelastic for bulge test

The bulge equations are mostly constructed for elastic materials, which are the main specimens used in bulge testing. However, it is not our case. Most of the stretchable substrates we used to make stretchable electronics are not elastic material. The material we used in the project, for example, PDMS, is an elastomer, which is a rubber-like, incompressible material. Thus we try to involve also hyper elasticity into the bulge test modelling, so as to better predict the PDMS membrane evolution during bulging.

3.2.1 Basic of hyperelasticity

Isotropic, continuum materials for which the constitutive behavior is merely a function of current state of deformation are known as elastic material, while for hyperelastic materials, the work done by the stresses during deformation process is dependent on the initial state and final configuration [27].

One can describe the constitutive behavior of a hyperelastic material using a strain energy function Ψ. Most of the strain energy functions are a function of invariants Ψ=Ψ(I_1, I_2, I_3), or sometimes, of stretches Ψ=Ψ($\lambda_1, \lambda_2, \lambda_3$). Noted that the Cartesian coordinates are used in the modelling, and the direction 1 is the direction along the window size, which we are mostly concerned. Stretches are what we are actually interested in, for it is the main cause of strain during bulge test. By definition, we know the stretch is the ratio of current length and the initial one: $\lambda = \frac{L_{current}}{L_{initial}}$.

For hyperelastic material, stresses are derived from the strain energy function Ψ. And for incompressible hyperelastic materials, the relations can be written as:

$$\sigma_1 = \frac{\lambda_1}{J}\frac{\partial \Psi}{\partial \lambda_1} - p$$

$$\sigma_2 = \frac{\lambda_2}{J}\frac{\partial \Psi}{\partial \lambda_2} - p$$

$$\sigma_3 = \frac{\lambda_3}{J}\frac{\partial \Psi}{\partial \lambda_3} - p$$

Here, $J = \lambda_1\lambda_2\lambda_3$, and is equal to 1 in the incompressible situations. p is the hydrostatic pressure induced by incompressibility.

σ_3 is the Cauchy stress component along the direction of membrane thickness. Due to boundary condition, $\sigma_3 = 0$. Thus, according to the last relation, we can tell that:

$$p = \sigma_3 = \frac{\lambda_3}{J}\frac{\partial \Psi}{\partial \lambda_3}$$

And the stress in plane can be write as:

$$\sigma_1 = \frac{\lambda_1}{J}\frac{\partial \Psi}{\partial \lambda_1} - p = \lambda_1\frac{\partial \Psi}{\partial \lambda_1} - \lambda_3\frac{\partial \Psi}{\partial \lambda_3}$$

$$\sigma_2 = \lambda_2\frac{\partial \Psi}{\partial \lambda_2} - p = \lambda_2\frac{\partial \Psi}{\partial \lambda_2} - \lambda_3\frac{\partial \Psi}{\partial \lambda_3}$$

σ_1 is equal to the in plane stress of the bulge membrane along the window size direction, and thus is the stress that mostly matters in the bulge equation.

In most cases, as mentioned before, strain energy function Ψ is a function of invariant, not stretch. Thus we need to recast the stress-energy relation by inducing the conversion of stretch and invariant:

$$I_1 = \lambda_1^2 + \lambda_2^2 + \lambda_3^2$$

$$I_2 = \lambda_1^2\lambda_2^2 + \lambda_2^2\lambda_3^2 + \lambda_1^2\lambda_3^2$$

$$I_3 = \lambda_1^2\lambda_2^2\lambda_3^2 = 1$$

The derivative of strain energy to a stretch component is used to calculate stress, and can be rewrite as:

$$\frac{\partial \Psi}{\partial \lambda_1} = \frac{\partial \Psi}{\partial \boldsymbol{I}}\frac{\partial \boldsymbol{I}}{\partial \lambda_1} = \frac{\partial \Psi}{\partial I_1}\cdot\frac{\partial I_1}{\partial \lambda_1} + \frac{\partial \Psi}{\partial I_2}\cdot\frac{\partial I_2}{\partial \lambda_1}$$

$$\frac{\partial \Psi}{\partial \lambda_2} = \frac{\partial \Psi}{\partial \boldsymbol{I}}\frac{\partial \boldsymbol{I}}{\partial \lambda_2} = \frac{\partial \Psi}{\partial I_1}\cdot\frac{\partial I_1}{\partial \lambda_2} + \frac{\partial \Psi}{\partial I_2}\cdot\frac{\partial I_2}{\partial \lambda_2}$$

$$\frac{\partial \Psi}{\partial \lambda_3} = \frac{\partial \Psi}{\partial \boldsymbol{I}} \frac{\partial \boldsymbol{I}}{\partial \lambda_3} = \frac{\partial \Psi}{\partial I_1} \cdot \frac{\partial I_1}{\partial \lambda_3} + \frac{\partial \Psi}{\partial I_2} \cdot \frac{\partial I_2}{\partial \lambda_3}$$

The derivatives of invariants to different stretches are:

$$\frac{\partial I_1}{\partial \lambda_1} = 2\lambda_1, \qquad \frac{\partial I_1}{\partial \lambda_2} = 2\lambda_2, \qquad \frac{\partial I_1}{\partial \lambda_3} = 2\lambda_3$$

$$\frac{\partial I_2}{\partial \lambda_1} = 2\lambda_1\lambda_2^2 + 2\lambda_1\lambda_3^2, \qquad \frac{\partial I_2}{\partial \lambda_2} = 2\lambda_2\lambda_1^2 + 2\lambda_2\lambda_3^2, \qquad \frac{\partial I_2}{\partial \lambda_3} = 2\lambda_3\lambda_1^2 + 2\lambda_3\lambda_2^2$$

So the derivative of strain energy function to a stretch component is:

$$\frac{\partial \Psi}{\partial \lambda_1} = \frac{\partial \Psi}{\partial I_1} \cdot \frac{\partial I_1}{\partial \lambda_1} + \frac{\partial \Psi}{\partial I_2} \cdot \frac{\partial I_2}{\partial \lambda_1} = \frac{\partial \Psi}{\partial I_1} \cdot 2\lambda_1 + \frac{\partial \Psi}{\partial I_2} \cdot (2\lambda_1\lambda_2^2 + 2\lambda_1\lambda_3^2)$$

$$\frac{\partial \Psi}{\partial \lambda_2} = \frac{\partial \Psi}{\partial I_1} \cdot \frac{\partial I_1}{\partial \lambda_2} + \frac{\partial \Psi}{\partial I_2} \cdot \frac{\partial I_2}{\partial \lambda_2} = \frac{\partial \Psi}{\partial I_1} \cdot 2\lambda_2 + \frac{\partial \Psi}{\partial I_2} \cdot (2\lambda_2\lambda_1^2 + 2\lambda_2\lambda_3^2)$$

$$\frac{\partial \Psi}{\partial \lambda_3} = \frac{\partial \Psi}{\partial I_1} \cdot \frac{\partial I_1}{\partial \lambda_3} + \frac{\partial \Psi}{\partial I_2} \cdot \frac{\partial I_2}{\partial \lambda_3} = \frac{\partial \Psi}{\partial I_1} \cdot 2\lambda_3 + \frac{\partial \Psi}{\partial I_2} \cdot (2\lambda_3\lambda_1^2 + 2\lambda_3\lambda_2^2)$$

Thus we can rewrite the stress-energy relationship as:

$$\begin{aligned}
\boldsymbol{\sigma_1} &= \lambda_1 \frac{\partial \Psi}{\partial \lambda_1} - \lambda_3 \frac{\partial \Psi}{\partial \lambda_3} \\
&= \lambda_1 \left[\frac{\partial \Psi}{\partial I_1} \cdot 2\lambda_1 + \frac{\partial \Psi}{\partial I_2} \cdot (2\lambda_1\lambda_2^2 + 2\lambda_1\lambda_3^2) \right] \\
&\quad - \lambda_3 \left[\frac{\partial \Psi}{\partial I_1} \cdot 2\lambda_3 + \frac{\partial \Psi}{\partial I_2} \cdot (2\lambda_3\lambda_1^2 + 2\lambda_3\lambda_2^2) \right] \\
&= \boldsymbol{\frac{\partial \Psi}{\partial I_1} \cdot 2(\lambda_1^2 - \lambda_3^2) + \frac{\partial \Psi}{\partial I_2} \cdot 2\lambda_2^2(\lambda_1^2 - \lambda_3^2)}
\end{aligned}$$

$$\boldsymbol{\sigma_2} = \lambda_2 \frac{\partial \Psi}{\partial \lambda_2} - \lambda_3 \frac{\partial \Psi}{\partial \lambda_3} = \boldsymbol{\frac{\partial \Psi}{\partial I_1} \cdot 2(\lambda_2^2 - \lambda_3^2) + \frac{\partial \Psi}{\partial I_2} \cdot 2\lambda_1^2(\lambda_2^2 - \lambda_3^2)}$$

We separate the derivative of invariants to stretches because they are the fixed terms for different strain-energy models. It is more convenient in actual computation.

3.2.2 Hyperelastic bulge modeling- geometrical general situation

The induction of constitutive behavior as a function of stretch into the modelling makes the significant difference from the original linear elastic model for bulge test. Our polymer substrate is an elastomer, when it deforms under bulging pressure, the work is done not only to perform plane strain or plane stress on the membrane, but may also cause thickness shrinkage which will then influence the bulge equation.

The geometry of a sector circular is used to calculate the strain of a bulge membrane in the window size direction, we first recall the section from chapter 2:

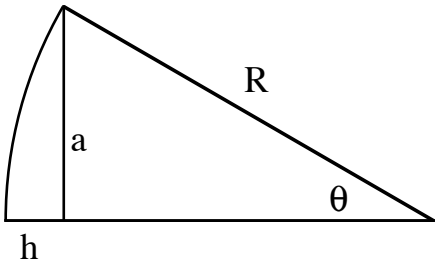

Fig.2.3. Schematic sketch of cross section of thin film and its geometry

$$R^2 = (R-h)^2 + a^2 = R^2 - 2Rh + h^2 + a^2 \approx R^2 - 2Rh + a^2$$

The assumption at last was made only on relatively small deflection, which may not hold any longer for an elastomer. To be more precise and general, one can write:

$R = (h^2 + a^2)/2h$

Like we mention before, to construct the pressure-deflection relation for hyperelastic case, stretch along window size direction should be considered here:

$\lambda_1 = R\theta/a$

θ, as can be seen from the geometry, is a function of R and a:

$\theta = \arcsin a/R = \arcsin 2ah/(a^2 + h^2)$.

Thus:

$$\boldsymbol{\lambda_1 = \frac{R\theta}{a} = \frac{h^2 + a^2}{2ah} \arcsin \frac{2ah}{a^2 + h^2}}$$

3.2.3 Hyperelastic bulge modeling- spherical window

As illustrated in the previous chapter, the stress in plane is equi-biaxial. Thus, when bulged, we can tell that $\sigma_1 = \sigma_2$, and the membrane is equally stretched along this two direction. That is: $\lambda_1 = \lambda_2$. The material we use, PDMS, is assumed to be incompressible, from this we know that $\lambda_1\lambda_2\lambda_3 = 1$, set $\lambda_1 = \lambda$, we get that:

$$\lambda_1 = \lambda, \qquad \lambda_2 = \lambda, \qquad \lambda_3 = \frac{1}{\lambda^2}$$

Use these results in the stress-stretch relation we obtained in previous section, we can get:

$$\boldsymbol{\sigma_1} = \frac{\partial \Psi}{\partial I_1} \cdot 2(\lambda_1^2 - \lambda_3^2) + \frac{\partial \Psi}{\partial I_2} \cdot 2\lambda_2^2(\lambda_1^2 - \lambda_3^2) = \mathbf{2}\frac{\boldsymbol{\partial \Psi}}{\boldsymbol{\partial I_1}}\left(\boldsymbol{\lambda^2} - \frac{\mathbf{1}}{\boldsymbol{\lambda^4}}\right) + \mathbf{2}\frac{\boldsymbol{\partial \Psi}}{\boldsymbol{\partial I_2}}\left(\boldsymbol{\lambda^4} - \frac{\mathbf{1}}{\boldsymbol{\lambda^2}}\right)$$

Recall the bulge equation for spherical windows from the previous chapter:

$$\sigma = \frac{pR}{2t} = \frac{p(a^2 + h^2)}{4th}$$

Here, $\sigma = \sigma_1$. Also, unlike in the linear elastic case, where thickness is a constant, in hyperelastic materials, thickness evolves as the bulge pressure build up, for we have a non trivial λ_3. If the original thickness is t_0, then the current thickness can be obtained as: $\boldsymbol{t = t_0 \cdot \lambda_3 = t_0/\lambda^2}$. So we can rewrite the previous equation as:

$$\boldsymbol{p} = \frac{4\sigma_1 th}{a^2 + h^2} = \mathbf{8} \cdot \frac{\boldsymbol{t_0 h}}{(\boldsymbol{a^2 + h^2})\boldsymbol{\lambda^2}} \cdot \left[\frac{\boldsymbol{\partial \Psi}}{\boldsymbol{\partial I_1}}\left(\boldsymbol{\lambda^2} - \frac{\mathbf{1}}{\boldsymbol{\lambda^4}}\right) + \mathbf{2}\frac{\boldsymbol{\partial \Psi}}{\boldsymbol{\partial I_2}}\left(\boldsymbol{\lambda^4} - \frac{\mathbf{1}}{\boldsymbol{\lambda^2}}\right)\right]$$

That is the bulge equation for hyperelastic material under spherical window. During the actual computation, one should substitute λ using the equation from last section:

$$\boldsymbol{\lambda} = \frac{\boldsymbol{h^2 + a^2}}{\boldsymbol{2ah}}\mathbf{arcsin}\,\frac{\boldsymbol{2ah}}{\boldsymbol{a^2 + h^2}}$$

3.2.4 Hyperelastic bulge modeling- rectangular window

For the rectangular window model, the plane-strain condition holds instead of equi-biaxial stress. That is $\varepsilon_1 \neq 0$， $\varepsilon_2 = 0$.

As refer to stretch, that means: $\lambda_1 \neq 1$， $\lambda_2 = 1$. Set $\lambda_1 = \lambda$， we get:

$$\lambda_1 = \lambda, \qquad \lambda_2 = 1, \qquad \lambda_3 = \frac{1}{\lambda}$$

We can use the stretch results in the stress-stretch relation and obtain:

$$\boldsymbol{\sigma_1} = \frac{\partial \Psi}{\partial I_1} \cdot 2(\lambda_1^2 - \lambda_3^2) + \frac{\partial \Psi}{\partial I_2} \cdot 2\lambda_2^2(\lambda_1^2 - \lambda_3^2) = \mathbf{2}\frac{\boldsymbol{\partial \Psi}}{\boldsymbol{\partial I_1}}\left(\boldsymbol{\lambda^2} - \frac{\mathbf{1}}{\boldsymbol{\lambda^2}}\right) + \mathbf{2}\frac{\boldsymbol{\partial \Psi}}{\boldsymbol{\partial I_2}}\left(\boldsymbol{\lambda^2} - \frac{\mathbf{1}}{\boldsymbol{\lambda^2}}\right)$$

$$= \mathbf{2}\left(\frac{\boldsymbol{\partial \Psi}}{\boldsymbol{\partial I_1}} + \frac{\boldsymbol{\partial \Psi}}{\boldsymbol{\partial I_2}}\right)\left(\boldsymbol{\lambda^2} - \frac{\mathbf{1}}{\boldsymbol{\lambda^2}}\right)$$

The bulge equation for rectangular window is:

$$\sigma = \frac{pR}{t} = \frac{p(a^2 + h^2)}{2th}$$

Like in the previous case, thickness changes as the bulge evolves. $\boldsymbol{t = t_0 \cdot \lambda_3 = t_0/\lambda.}$

Thus the bulge equation for hyperelastic material under rectangular window is:

$$\boldsymbol{p} = \frac{2\sigma_1 th}{a^2 + h^2} = \mathbf{4} \cdot \frac{\boldsymbol{t_0 h}}{\boldsymbol{(a^2 + h^2)\lambda}} \cdot \left(\frac{\boldsymbol{\partial \Psi}}{\boldsymbol{\partial I_1}} + \frac{\boldsymbol{\partial \Psi}}{\boldsymbol{\partial I_2}}\right)\left(\boldsymbol{\lambda^2} - \frac{\mathbf{1}}{\boldsymbol{\lambda^2}}\right)$$

Here, the substitution of stretch to window size and deflection height still holds:

$$\boldsymbol{\lambda} = \frac{\boldsymbol{h^2 + a^2}}{\boldsymbol{2ah}} \mathbf{arcsin}\ \frac{\boldsymbol{2ah}}{\boldsymbol{a^2 + h^2}}$$

3.2.5 Hyperelastic bulge modeling- with constitutive modeling

We obtained the bulge equation for hyperelastic material in the previous section. The strain energy function is given by different constitutive models, thus to finish the modeling, we induce the most commonly used constitutive models for hyperelastic rubber like materials.

For the hyperelastic bulge equations, the constitutive models change only the derivative of strain energy and invariant. To be less tedious, only $\frac{\partial \Psi}{\partial I_1}$ and $\frac{\partial \Psi}{\partial I_2}$ would be listed for each model. Noted that the models listed below are already simplified by considering only the incompressible situation. While doing actual the computation, one should substitute the derivatives of the desired model to the bulge equation listed in the previous section.

Uniaxial stress-stretch relation

First we want to write the stress-stretch relation for uniaxial cases, for it can be an alternative source of constitutive behavior of material and shows and other possibility to use this model. One can perform a uniaxial tensile test on the substrate material, the curve can be fitted computationally by MATLAB to obtain the material parameters. And then, one can use the parameters into the hyperelastic bulge equations to relate the pressure and strain, so as to study the strain history on the bulged membrane.

Recall from previous section, the general stress-stretch relation is:

$$\sigma_1 = \frac{\partial \Psi}{\partial I_1} \cdot 2(\lambda_1^2 - \lambda_3^2) + \frac{\partial \Psi}{\partial I_2} \cdot 2\lambda_2^2(\lambda_1^2 - \lambda_3^2)$$

But for uniaxial stress, the membrane will be stretch one-dimensionally, and contracts on the rest two dimensions. That is to say:

$$\lambda_1 = \lambda, \qquad \lambda_2 = \frac{1}{\sqrt{\lambda}}, \qquad \lambda_3 = \frac{1}{\sqrt{\lambda}}$$

So the stress-stretch relation is:

$$\boldsymbol{\sigma_1 = 2\frac{\partial \Psi}{\partial I_1}\left(\lambda^2 - \frac{1}{\lambda}\right) + 2\frac{\partial \Psi}{\partial I_2}\left(\lambda - \frac{1}{\lambda^2}\right)}$$

General terms for different constrain situation

The bulge equation for hyperelastic material have terms that change for different cases-the invariants. Invariant is a function of stretch, and as can be seen above, stretch differs from case to case. Thus here listed the invariants according to different cases. When using the hyperelastic bulge equation, one should put the proper substitution to invariants according to the actual case.

1) Spherical window case-equibiaixial situation

$$\lambda_1 = \lambda, \qquad \lambda_2 = \lambda, \qquad \lambda_3 = \frac{1}{\lambda^2}$$

$$\boldsymbol{I_1 = \lambda_1^2 + \lambda_2^2 + \lambda_3^2 = 2\lambda^2 + \frac{1}{\lambda^4}}$$

$$\boldsymbol{I_2 = \lambda_1^2\lambda_2^2 + \lambda_2^2\lambda_3^2 + \lambda_1^2\lambda_3^2 = \lambda^4 + \frac{2}{\lambda^2}}$$

2) Rectangular window case-plane strain situation

$$\lambda_1 = \lambda, \qquad \lambda_2 = 1, \qquad \lambda_3 = \frac{1}{\lambda}$$

$$\boldsymbol{I_1 = \lambda_1^2 + \lambda_2^2 + \lambda_3^2 = \lambda^2 + 1 + \frac{1}{\lambda^2}}$$

$$\boldsymbol{I_2 = \lambda_1^2\lambda_2^2 + \lambda_2^2\lambda_3^2 + \lambda_1^2\lambda_3^2 = \lambda^2 + \frac{1}{\lambda^2} + 1}$$

3) Uniaxial situation (for fitting)

$$\lambda_1 = \lambda, \qquad \lambda_2 = \frac{1}{\sqrt{\lambda}}, \qquad \lambda_3 = \frac{1}{\sqrt{\lambda}}$$

$$\boldsymbol{I_1} = \lambda_1^2 + \lambda_2^2 + \lambda_3^2 = \boldsymbol{\lambda^2 + 2/\lambda}$$

$$\boldsymbol{I_2} = \lambda_1^2\lambda_2^2 + \lambda_2^2\lambda_3^2 + \lambda_1^2\lambda_3^2 = \boldsymbol{2\lambda + \frac{1}{\lambda}}$$

Arruda-Boyce form

$$\Psi = \mu\left[\frac{1}{2}(I_1 - 3) + \frac{1}{20\lambda_m^2}(I_1^2 - 9) + \frac{11}{1050\lambda_m^4}(I_1^3 - 27) + \frac{19}{7000\lambda_m^6}(I_1^4 - 81) + \frac{519}{673750\lambda_m^8}(I_1^5 - 243)\right]$$

$$\frac{\partial\Psi}{\partial I_1} = \mu\left(\frac{1}{2} + \frac{2}{20\lambda_m^2}I_1 + \frac{11\times3}{1050\lambda_m^4}I_1^2 + \frac{19\times4}{7000\lambda_m^6}I_1^3 + \frac{519\times5}{673750\lambda_m^8}I_1^4\right)$$

Here, μ, λ_m are temperature dependent material parameters.

Mooney-Rivlin form

$$\Psi = C_{10}(I_1 - 3) + C_{01}(I_2 - 3)$$

$$\frac{\partial\Psi}{\partial I_1} = C_{10}, \qquad \frac{\partial\Psi}{\partial I_2} = C_{01}$$

Neo-Hookean form

$$\Psi = C_{10}(I_1 - 3)$$

$$\frac{\partial\Psi}{\partial I_1} = C_{10}$$

Polynomial form (N=2)

$$\Psi = \sum_{i+j=1}^{N} C_{ij}(I_1 - 3)^i\,(I_2 - 3)^j$$

$$\frac{\partial \Psi}{\partial I_1} = C_{10} + C_{11}(I_2 - 3) + 2C_{20}(I_1 - 3)$$

$$\frac{\partial \Psi}{\partial I_2} = C_{01} + C_{11}(I_1 - 3) + 2C_{02}(I_2 - 3)$$

Yeoh form

$$\Psi = C_{10}(I_1 - 3) + C_{20}(I_1 - 3)^2 + C_{30}(I_1 - 3)^3$$

$$\frac{\partial \Psi}{\partial I_1} = C_{10} + 2C_{20}(I_1 - 3) + 3C_{30}(I_1 - 3)^2$$

3.2.6 Conclusion and discussion

We begin with with the original bulge equations, showing curves of pressure-deflection relation with different window size and under different constrain situation. But these relations hold only for elastic materials. Then we try to build the numerical model on bulge test for our stretchable substrate, which is an elastomer, that may not comply to the original bulge equation developed for linear elastic materials.

By referring back to the original bulge equations, we find that the equation is constructed on the assumption of small deflection at the geometrical modelling. Thus we rewrite the rewrite the strain relationship with window size and deflection height. Only this time we use stretch instead of strain, for it gives more meaning in hyperelasticity. Stretch along window size direction is thus obtained with a more expended function. This relationship is used to substitute the stretch in the hyperelastic bulge equation.

According to hyperelasticity, stress can be written as a function of stretch and derivative of strain energy and invariant. Thus we express the in-plane stress with derivatives of strain energy and invariants, as well as stretch.

Bulge equation is then reconstructed using the updated stress equation. Thickness evolution is also considered by replacing a constant thickness to a stretch-dependent one.

Constitutive models for rubber like hyperelastic materials are induced to complete the modeling. Only the derivatives of strain energy and invariant differ model by model, thus only this part is listed. In actual application of hyperelastic bulge equation, one should substitute different parts with corresponding equations according to the specific constrain situation.

Uniaxial tensile stress is also mentioned in this chapter, for the possible application in experimental cooperation. One can perform a uniaixial tensile test on the same material that would be use in bulge device, fit the data with hyperelastic model to give parameters and then used in the next step. It is an optional way to obtain material properties experimentally and thus to give a better reference to pressure-strain relationship, which serves our goal. Another way to achieve this is using the profilometer, by controlling the pressure we get different profiles and thus different deflection height. We can use the p-h curve to directly fit the models and to give reference to the strain history of crack opening study. This methodology will be illustrated later.

While building the model, we try to obtain material parameters from Abaqus auto-fitting and MATLAB using the experimental uniaxial tensile data to do comparison. Using the Abaqus fitted parameters to fit the modeling of hyperelastic bulge equation, we found that though the reconstructed stress-strain curves seemed fitted well in the uniaxial case, it shifted a lot in the equi-biaxial case. We recommend to use the same software to obtain parameters so as to minimize the systemic error.

Taking advantage of the fact that minor deviation of parameter fitting in the uniaxial case can cause huge shift in biaxial situation, one can also use this model to identify a more appropriate hyperelastic constitutive model to focus on.

4 Development of the bulge test setup

We fabricate a device setup to perform bulge test on our stretchable membrane. During the development of the setup, we encounter different issues and several modification and prototypes were made before the final version of the device. Here we will just illustrate the final version of our device setup, and point out some key issues that need to be considered during the manufacture.

The window of our bulge device is a spherical window, 1mm in diameter. We choose only the spherical window, for the reason that it has a better-known theoretical backup compared to square window, and that it is more suitable for elastomer, while the plane strain condition in the rectangular window is more favored by a much stiffer material.

The possible pressure range the bulge test setup can provide is 0-1.5 PSI.
REASONING OF THE SETUP: CHARACTERIZATION; OBSERVE CRACKING BEHAVIOUR UPON EQUI-BIAIXIAL

4.1 Sample preparation [28]

The gold on PDMS samples we used in our experiment are fabricated by Tinku et al. in Fondazione Bruno Kessler. (IS IT OK TO WRITE LIKE THIS?) So here we just give brief introduction of the material properties and the fabrication techniques. A detail fabrication reference is listed in the bibliography [28] and the characterization of the sample in [29].

PDMS has a significantly different thermal expansion coefficient than the rest of the layers in the micro fabrication routine. This may lead to lots of cracks and adhesion issues. Thus special caution should be paid to minimize the thermal shocks steps during the process. The direct contact of PDMS and photoresist was first avoided, so as to avoid thermal shocks to the polymer.

The fabrication steps were as follows: Cleaning and rinsing of the wafers- Silanization of the wafers for easy removal of PDMS- PDMS (10:1 ratio) coated on wafer at 500 RPM for 60 sec.(thickness of PDMS~150μm) - Coated wafer kept 2 hours in oven at 80°C for polymer curing- Oxygen plasma to modify the surface adhesion- E-beam evaporation- 10 nm Ti and 100nm Au is deposited all over wafer- A positive photoresist coated on Au layer- Patterned photoresist by UV treatment- Etching on Au and Ti- Removal of remaining photoresist- PDMS peeled from Si wafer- Molding

PDMS. The optimized fabrication techniques and the steps are illustrated in the following figure.

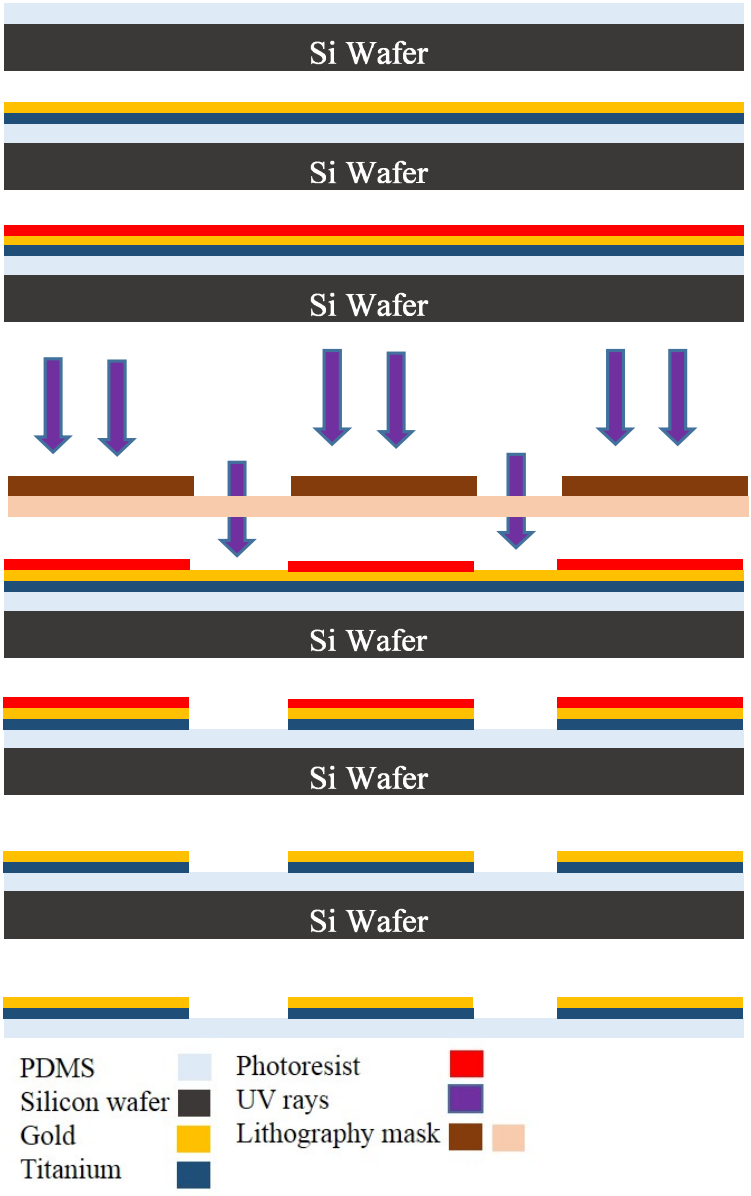

Fig.4.1. Optimized micro fabrication steps for metal patterning on PDMS

4.2 Device Manufacture

The main body of the device is manufactured in the micro workshop of LabS in Politecnico di Milano. The component choice of the device and its size are decided with main consideration of the possession and precision the workshop can provide, combined with the availability of that element in online market.

4.2.1 Overview of setup

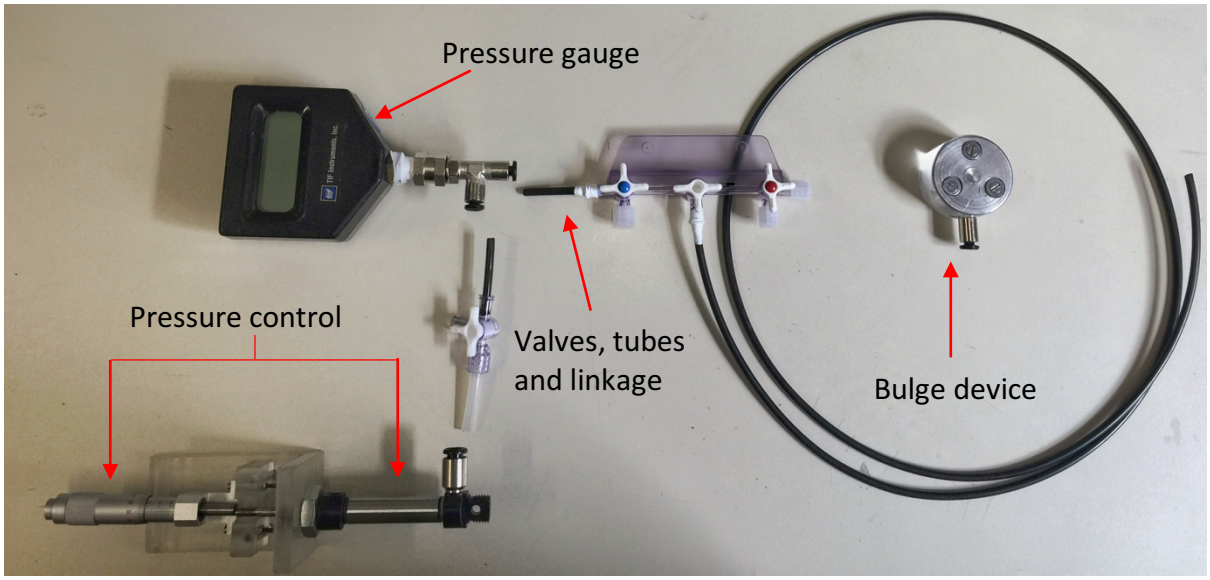

Fig.4.2. Overall setup of bulge test

The overall bulge test setup is shown in Fig.4.2. The most important components are: pressure provider system, pressure sensor, linkage system and the bulge device.

Normal pressure providing system for bulge test can be divided into two groups: gas provider and liquid provider. Liquid provider are used too meet larger pressure requirement for stiffer materials, which is not our case. Also, the filling procedure and air entrapment problem are significant to liquid provider system. Thus we choose gas to be the pressure provider. It is more available, the possible pressure range is enough to inflate an elastomer. A cylinder of compressed air plus a micro-screwer are used in

our setup. A syringe, which is not shown in the picture, is used to pump in air wile the whole range of cylinder is compressed. It will be illustrated in the later sections.

For pressure sensor, a pressure gauge from TIF Instruments Inc. is used. The measuring unit is psi, with range 0-99.99.

The linkage system is carried out by two plastic valves and several tubes. Two valves are used to separate the pressure providing system or the bulge test device, so that one would not affect the other, while repumping air, or while during test. Tubes should be as small as possible and as short as possible, for a more effective compression of air. However, the tube that connects to the bulge device is long, for the reason to keep bulge device farther away and thus less affected during the manipulation of pressure.

Fig 4.3. shows the overview of the bulge test device. Details will be shown later.

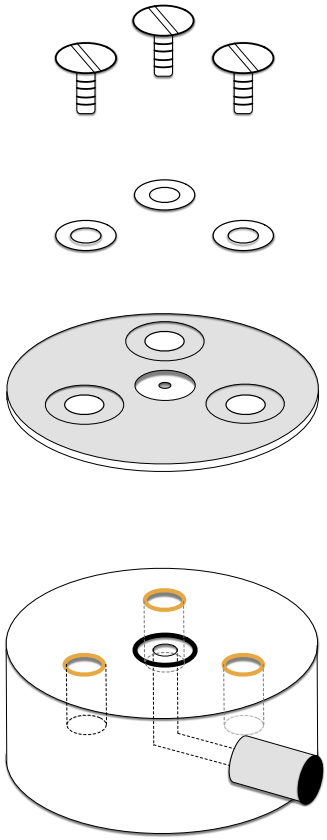

Fig.4.3. Overview of bulge test device

4.2.2 Cap manufacturing

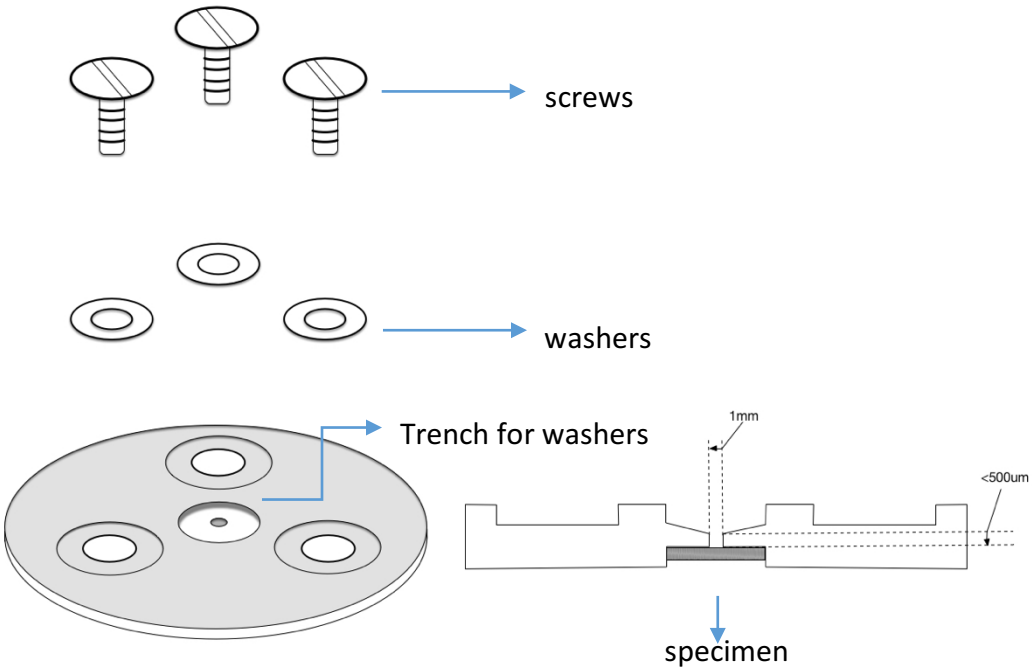

Fig.4.4. Schematic illustration of cap alignment

The schematic illustration of cap alignment is shown in Fig.4.4. The alignment includes: screws, washers and the cap. Only spherical windows are made during this project, for the reason that rectangular windows provide constrains for plane strain condition, which will be more suitable for stiffer materials. But one can fabricate rectangular or even square windows under similar fabrication procedure.

The cap is fabricated from a piece of metal with thickness less than 2mm. In the central region of the cap, an opening is fabricated to reduce the depth from the top to the specimen, so that the device is applicable for experiment under laser profilometer. The laser profilometer has a working distance below 1.5mm, a slope of the opening is made on purpose to allow the laser head to approach closer to the specimen without hitting the outer fringe.

Once the membrane is detected, the laser head moves up and down in the distance of 500 microns, to determine its position. So the distance between the top of opening and

the specimen at unbulged condition should be less than 500 microns. But it is difficult to achieve on a single side fabrication, otherwise the slop is too large. The specimen stage on the backside of the cap is made for this purpose. The diameter of the stage can be fix to the value of that of the specimen, such that it is easier to center the specimen.

Only a window of 1mm in diameter is made as a metal cap, though we tried out several caps with other window sizes from PMMA. We choose finally metal instead of PMMA like the rest of the device, to ensure the compatibility with the screws head, otherwise the cap would be blended after a few times of usage.

Three trenches for washers are fabricated also on the cap. The usage of washer increases the tightening of the screw head and the cap, which then ensures a better sealing condition. The central holes of the washers are shaped slightly conically, so as to fit the screw heads even better. But this depends on the type of screws that would be used in the device. We choose the screws with conical heads. The finished product is shown in Fig.4.5.

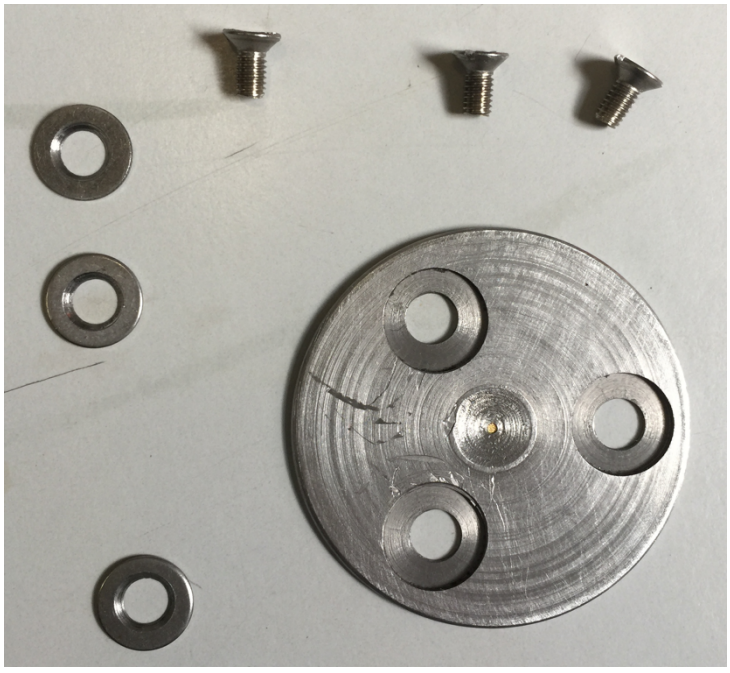

Fig.4.5. Finished product of cap

4.2.3 Main body manufacturing

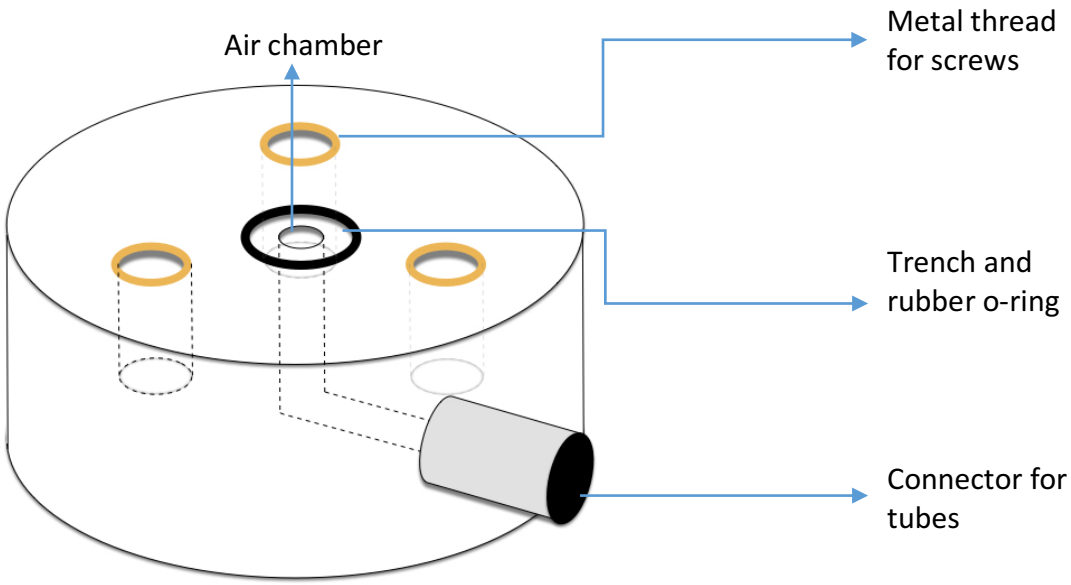

Fig.4.6. Schematic illustration of device chamber

The schematic illustration of the main body of the device is shown in Fig.4.6. The device is fabricated with PMMA, which is a cheap, environmental friendly material. The main body of the device include several important components, those are: air chamber, trench and o-ring, metal thread for screws and the connector for tubes.

The device is made as a cylinder, and the air chamber is constructed in the center. It is mainly for the easiness for fabrication. Air chamber does not have size limitation, due to the fact that window constrain is provided by the cap instead. But in order to have more effective pressure build up, the chamber should not be too big.

The bottom of the cylindrical chamber links to connector for tubes. It is a metal component with o-rings on the thread and it is purchased online. It provides excellent sealing. A plateau and a thread hole is manufactured in the PMMA main body, to accommodate the connector even better.

A trench outside the air chamber is fabricated for the placement of an o-ring. The o-ring is needed to improve sealing ability. The trench should be half of the o-ring

thickness in depth, and slightly smaller than the o-ring in diameter and width. While the o-ring is being placed, it should be a little bit stretched spherically and compressed along width so as to be fixed at the position. When fixing the cap on top, the o-ring should be compressed drastically and no space should exist between cap and device.

The threads for screws are made from metal, and purchased online. At first we directly drilled threads for screws on the PMMA main body, but after a few times of fix-unfix of screws, the threads seemed to be lost. We used an extra piece of metal thread to increase the compatibility of screws and the main body of the device. The metal threads are fixed into the PMMA once it is placed. The size of the threads depends on that of the screws.

Fig.4.7. shows the finished product of the main body of the device.

Fig.4.7. Finished product of main body of the device

4.2.4 Pressure build up and control

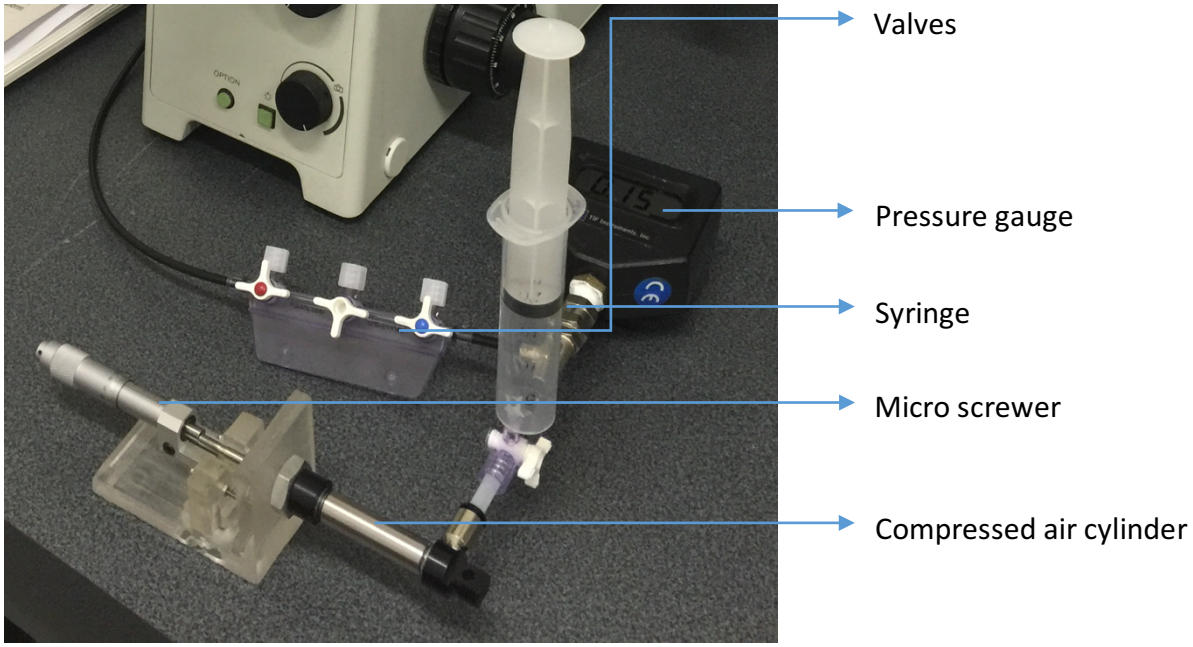

Fig.4.8. Actual setup of pressure providing and controlling system

The pressure build-up and control system is one of the main part of the overall setup. It contains several components: syringe and compressed air cylinder works as pressure provider; pressure gauge as pressure sensor, valves and micro screwer as pressure controller. The general idea is to provide pressure by compressing air.

For pressure providing system, the syringe is the main air provider. We use it to pump in air to a certain value, and close the valve on its side. Then a compressed air chamber cylinder is used to adjust gradually the pressure until it reaches the one desired. We used a micro screwer to push the piston. The compressed air cylinder is bought from Air Work Pneumatic Equipment. The construction of the cylinder is shown in Fig.4.9., the larger chamber is used, for that small chamber provide pressure higher than necessary, and it is unstable.

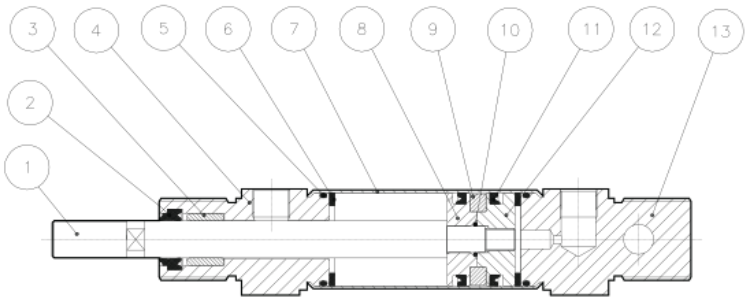

pos.	descrizione / description
1	stelo / rod
2	guarnizione stelo / rod seal
3	bussola guida / guide bush
4	testata anteriore / front cap
5	o-ring
6	paracolpo / bumper
7	tubo / tube
8	pistone / piston
9	magnete / magnet
10	o-ring
11	guarnizione pist. / seal piston
12	pistone / piston
13	testata posteriore / rear cap

Fig.4.9. Construction of the compressed air cylinder

For pressure sensing, a pressure gauge from TIF Instrument Inc. is used. The pressure gauge measures the pressure in the unit of PSI (1 PSI~ 6.9 kPa). The measuring range is from 0.00-99.99 PSI, with resolution of 0.01 PSI. The hexnut of the pressure gauge must be tightened while mounting to the system, and some white tape should be applied on the thread, in order to improve the sealing.

For pressure controlling system, several valves and a micro screwer is involved. In aspect of the micro screwer, it is used not only to push the piston of the compressed air chamber cylinder, but also to finitely adjust pressure. The position of the piston is fixed thus not rebouncable by the micro screwer, such that pressure of the system can hold at a stable condition. Two three-way valves are also used to better control the pressure and avoid leakage as much as possible.

One of them is placed at the joint of device and pressure gauge (valve 1), the other is at the joint of pressure gauge and the pumping system (valve 2), that is, the syringe and air compressed chamber cylinder. During the air-repumping by the syringe when the full range of piston runs out, the valve 1 should be closed to the bulge device, pressure gauge and the pressure providing system remains linked. While adjusting finitely the pressure, the side of syringe should be closed, and after that, the whole pressure providing system should be isolated by turning off valve 2. In this way, the possible leakage from the providing system can be completely avoided during bulge test.

4.3 Specimen preparation and mounting

Fig.4.10. A specimen mounted on the specimen stage of the backside of cap

The specimen includes a small piece of sample and a tape to hold it beneath the cap.

The fabrication on the tape is very important. The tape is a double sided tape, the top side is for adhesion to the cap, the bottom side is for sticking the gold on PDMS sample. It is drilled out a hole at center, with diameter exactly as that of the cap window size. The overall size of the cap is roughly the same as that of the specimen stage. To be as precise as possible, especially on the centrality and the size of the window hole, laser cut is used to fabricate the tape. A thorough hole and a fringe mark is made on the tape. Fig 4.11. shows the finished tape after laser cut.

After handling of the tape, it is cut out around the mark, or punched out by a puncher with the same diameter. The alignment of the cap and the tape is crucial, the window of the cap is exactly where the hole of the tape should be located. In order to do this, we used a needle of 1mm in diameter, fix it on a stage, and put firstly the cap then the

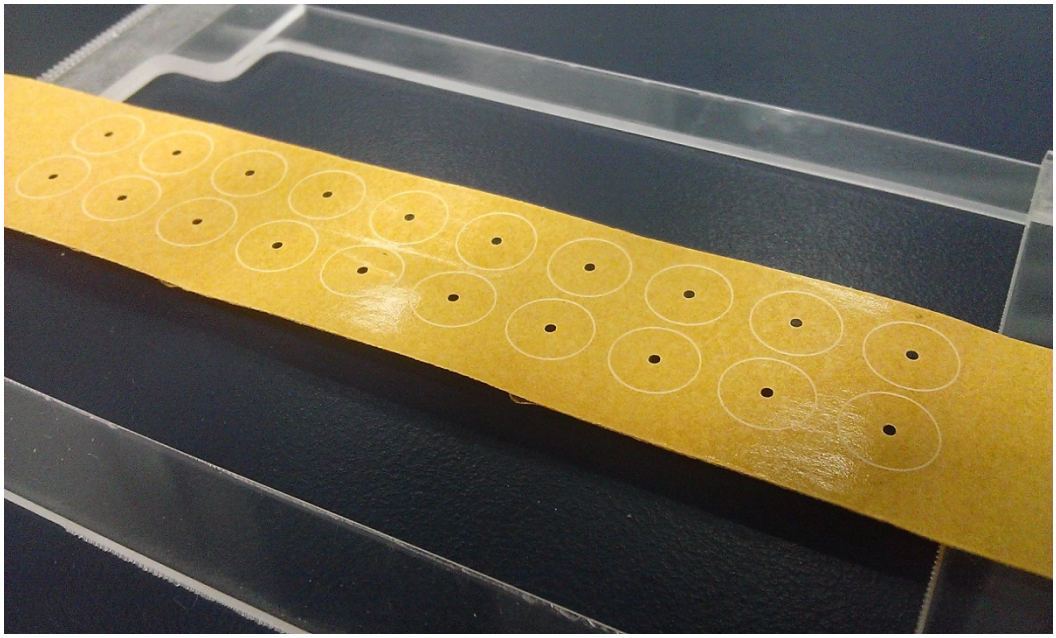

Fig.4.11. Laser cut and marked double layer tape

tape, with the sticky side facing the backside of the cap. One should be as careful as possible, using the tweezers to gradually approach the cap. Once the tape and the cap is centralized and the holes are matched up, we remove the cap from the needle, and use a flat head screw to punch a bit on the backside of the tape, to ensure a good adhesion to the cap.

After sticking the tape to the cap, one can peel out the protective layer on the backside of the tape. A small gold on PDMS sample should be then mounted on the tape. In fact, the sample does not have an exact limitation in size, though in aspect of saving material, the smaller the better, as long as it is big enough to cover the window hole. While peeling out the sample from the silicon substrate, one should do it slowly and gradually, in order to avoid inducing new cracks in the deposited gold layer. The sample should be facing the tape with the gold coated side.

After all alignment of the specimen, the cap should be closed up by fixing in the screws. Special caution should be paid to the storage of the cap while the specimen is mounted on the cap but not on the device yet. Mechanical damage and chemical contamination should be avoid.

4.4 Effort to improve sealing

Sealing is vital for the whole bulge test device setup. Leakage should be reduced to an ignorable extent, if not completely eliminated. The reason we need to avoid leakage is that, if once there were some unsealed part, the air will leak out, either rapidly or gradually, the pressure inside the setup will drop, which will lead to an unstable loading to the test membrane. No stress nor strain can be controlled in this situation. Here we will illustrate the special attention paid to the sealing problem on the device and on the pressure providing and controlling system.

4.4.1 Sealing on the device

The first effort to ensure the sealing on the device, is the usage of tape in the specimen. We tried several tapes to find the most adhering one. After placing the tape into the specimen stage, we use flat head screw to punch the tape to achieve maximum adhesion between the tape and the cap. We do the same after the mounting of the sample. The sample should be cut a bit bigger than the window hole, to leave enough arear for adhesion to the tape. We place the sample beneath the window, not above it, because while bulged, the latter case shows delamination between the tape and the sample. It is what we do not want during bulge test.

The second detail design for sealing is the usage of metal cap. A metal cap is used instead of a PMMA one, due to the fact that PMMA caps blend easily after a few attempts of fix-unfix screws. If blended, there would leave a space between cap and the device, and it induce leakage.

Conically shaped washers are used to better avoid the blending of the cap and improve the tightening of the cap and the screws. Trenches are fabricated to accommodate the washers. While tightening the screws, one should go step by step, instead of fixing

totally one in than the others, to avoid blending. The conical shape of the hole of washer allows screws to fix completely in to provide the best tightening by its head.

A metal thread is placed inside the device for the screws, such that after long time usage the thread will not fade out. In our previous prototype this problem happens. The screws can not fix in totally once the thread is lost.

A trench for o-ring is fabricated on the device, slightly larger than the specimen chamber size. The trench is as deep as half of the o-ring thickness, and slightly smaller than it in size. The reason for this fabrication, as we mentioned before, is to fix the o-ring exactly where it is supposed to be, so when compressed, it would not move. When fixing the cap on top, the o-ring will be compressed until there exist no observable space between the cap and the device. Further leakage is locked back by the o-ring.

The connector for tubes has also an o-ring on the thread which is used to fix in the device. The connection part for tubes is made from rubber. When inserting a tube, one should press the rubber piece to the bottom then release. In such manner the sealing between the tube and the connector is ensured.

4.4.2 Sealing on the pressure providing and controlling system

The first to be mention is the isolation between the pressure providing system and the device-sensor alignment. Though it is not strictly necessary, reducing components linked to the device during tests is beneficial. In this case, leakage can be avoided even if it exists in the compressed air chamber cylinder.

Next to be mentioned about is the pressure gauge. We experienced a slight leakage on the pressure gauge, thus one should not ignore this instrument. The hexnuts of the gauge should be all tightened up. The thread that connects the gauge and the metal joint component should be covered up by white tape to guarantee the sealing.

Last but not least, the valves. All the valves should be turned to the exact position. Also, when connecting the tubes to the valves, white tapes are used to wrap the joint, so that leakage is prevented.

4.4.3 Conclusion and discussion

Sealing should be checked before any experiment. Either laser profilometer or inverted microscope takes time to scan or to obtain images. This requires the membrane to be stable at a fixed pressure load.

One can build up pressure and leave the whole setup as it is for around ten minutes. If the pressure drops slightly, it is acceptable, otherwise one should check the sealing component by component. If there is leakage, it will be more drastic under higher pressure. So one can build up high pressure to rapidly check the sealing. However, if the specimen is used for studying the crack opening under inverted microscope, the sealing should be checked at very low pressure, otherwise it might induce new cracks that might influence our study. The specimen for profilometer does not holds the same problem. And the sealing is more crucial in those test thus should be ensured.

5 Bulge test with in-situ laser profilometry

To study crack opening corresponding to strain history of the gold on PDMS membrane, we should have control on strain loading. The realization of bulge test device enables us to do so by manipulating applied pressure and constraining window size. As was mentioned in the theoretical chapter, the deflection height of the bulged membrane is a direct consequence of internal pressure, but from the bulge equation modelling we can derive the corresponding strain. Thus, to understand how the strain loading is controlled, we should first get the p-h relation of our bulge device.

A laser profilometer can help us to achieve our purpose. We perform the experimental test under laser profilometer, to obtain membrane profile under each specific pressure. By abstracting the deflection height from the profile and relate it to pressure, we get the desired p-h relation. The strain loading control then can be fully understood and is ready to apply on the crack opening study under in-situ optical microscopy.

5.1 Introduction of laser profilometry [30]

A laser profilometer is generally used for quantitative recognition and recording of micro-topography of a surface. The working principle of the laser profilometer relies on determining the relative distance by searching for the focus point.

An infra-red laser is produced from a semiconductor and focused to a spot by an objective lens. The size of the spot and sensor stand-off depend on the numerical aperture of the lens. The greater the numerical aperture, the smaller diameter of the focused beam, and the smaller working distance.

The laser is directed to the sample being measured, then reflected. The reflected light is then directed to a prism by a beam splitter, after which the laser is imaged as a pair of spots on a set of photodiodes that are not arranged at the moment.

The setup is then arranged. When both diodes are equally illuminating, it indicates the precise focus distance from the sample. As a consequence, if the distance between the sample and the objective lens changes by a certain amount, the imaged focus point will be changed and the illumination of the diodes will no longer be equal.

This results in a focus measurement error that is generated by a differential amplifier. In order to perform an accurate measurement, both the spot size and its subsequent light distribution must be kept as constant.

A control circuit is used to manage this. It monitors the focus error and moves the objective lens according to the feedback changes in the distance between objective lens and sample. The objective lens are moved by a coil and magnet arrangement. Movement is recorded by a light barrier measurement system which then yield the change of focal distance over the sample surface, that is, the sample topography.

The instrument we used in our measurement is an UBM Laser Profilometry. The specifications of the particular used instrument are as follows: a linear spot of diameter of 1μm, a tolerable inclination of ±15°, a measurement range ±500μm, and a vertical resolution 10nm. The illustration of the measurement principles is shown in Fig.5.1.

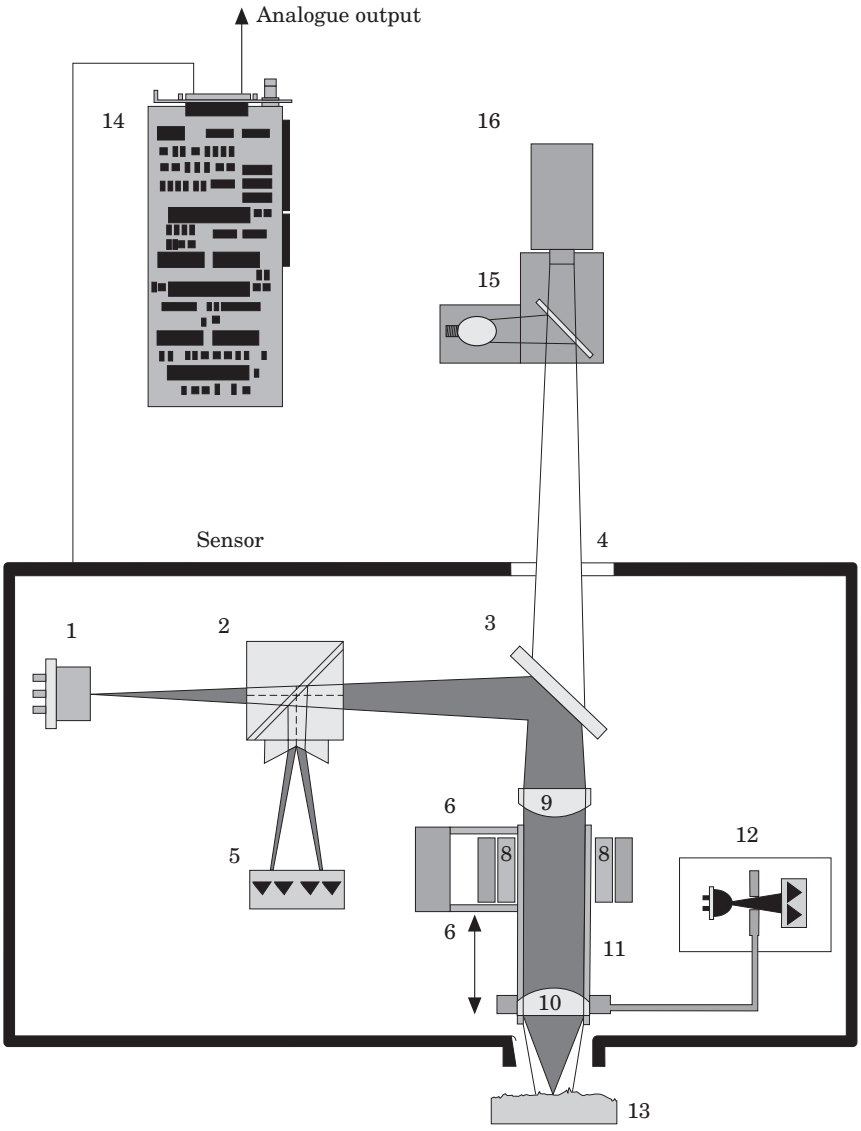

Fig.5.1. Illustration of the measurement principle of the UBM laser profilometer. (1) Laser diode, (2) prism with beam splitter, (3) beam splitter, (4) window, (5) photodiodes, (6) leaf spring, (7) coil, (8) magnet, (9) collimator lens, (10) objective, (11) tube, (12) light barrier measurement system, (13) measurement object, (14) PC board, (15) microscope with illumination, (16) CCD camera.

5.2 Setup description

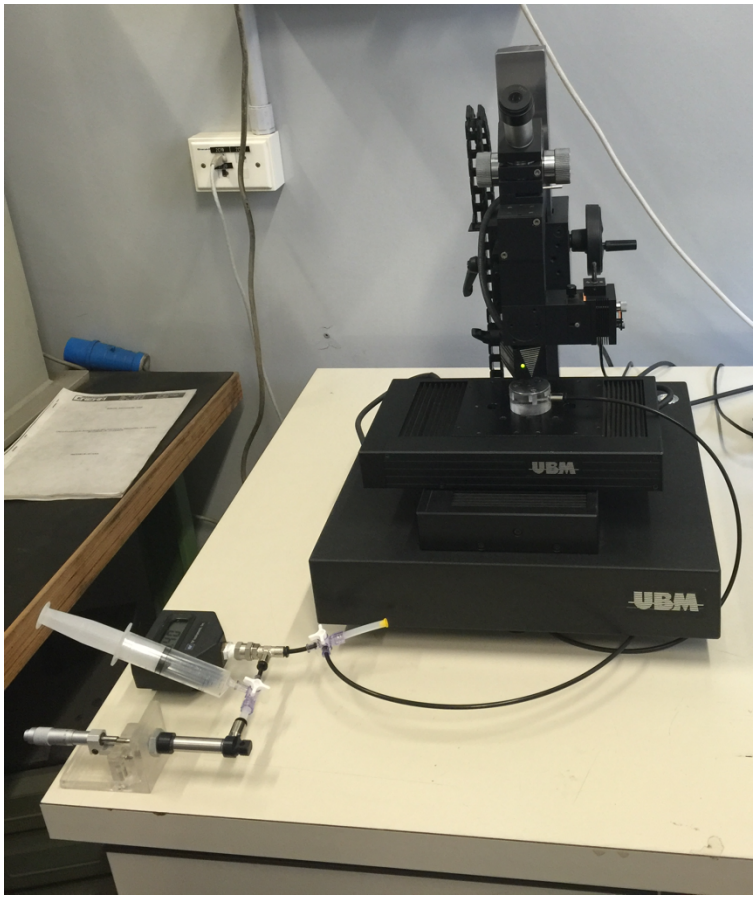

Fig.5.2. Experimental setup for bulge test with in-situ profilometry

The overall setup is shown in Fig.5.2. There are several key points that need to be mentioned.

Firstly, the bulge device should be firmly fixed on the working stage. Once the actual region to be measured is determined, that region should be fix in position so that a profile of surface can be obtained due to an effective scan. Secondly, the device should be linked to the rest pressure providing and controlling system with a long tube. In this manner, the manipulation of the microscrewer and the syringe pump will not influence significantly the device. Thirdly, the pressure gauge and the microscrewer stage can be stuck on the desk to further reduce the possible vibration during manipulation.

5.3 Experiment Protocol

The experiment is conducted under the following protocol:

1) Align the bulge test setup as illustrated in Chapter 4.

2) Check the sealing condition of the device.
   The scanning to obtain the profile of a region of membrane takes relatively long, thus the pressure should maintain stable.

3) Align the experimental setup as illustrated in 5.2.
   Make sure that the device is firmly fixed on the working stage.

4) Choose non-continuous mode with 400μm*400μm observation window. Bulge the sample to 0.15 PSI. Focus on central bulged region.
   Non-continuous mode is chosen, because the measurement under continuous mode lost a large amount of data point.
   However, it is a very slow mode, we try to conduct a non-continuous mode on full-field of bulge window, it takes around 30 min to obtain profile for a single pressure value. Thus we decide to focus only at the central region with observation area of 400μm*400μm.
   It is not easy to locate the central region that will be bulged while the membrane remains at rest. In order to determine the concerned region, we apply a small pressure to bulge the membrane. The central bulged region is obvious and thus can be locked up.

5) Release the pressure to zero, obtain the first profile data, record as 0 pressure.
   It is the initial data point of our experiment.

6) Increase pressure at interval of 0.05 PSI until it reaches 0.5, record profile for each pressure.

As we can indicate from the p-h curve shown in Chapter 3, at the beginning, a small increment of pressure results in considerable deflection. So the data points at the beginning should be denser.

7) Increase pressure at interval of 0.1 PSI, until it reaches 1, record profile for each pressure.

It takes a larger pressure increment to obtain the same deflection change as at the beginning. We can save sometime and will not loose lots of information by doubling the increment interval.

8) Synthesis the profile data.

An example of synthesized data is shown as follows.

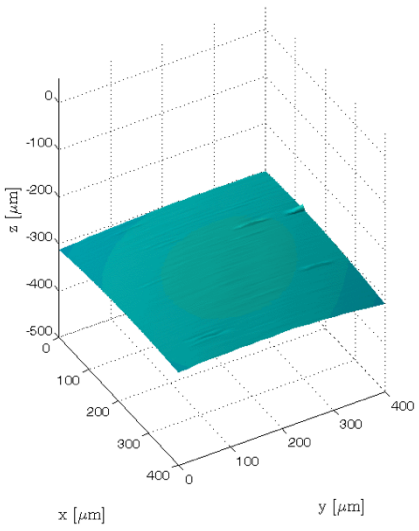

Fig.5.3. Example of synthesized data

9) Post-Processing.

It will be illustrated in the next section.

5.4 Results and discussion

Df

(1) Post-processing

(2) Experimental curve result---enables the crack opening study, a-dependent…

(3) Size dependent--Experimental Characterization combined with hyperelastic modeling-equibiaxial case- FITTING, parameters, ect…---a-independent//characterization of the material.

6 Bulge test with in-situ optical microscopy

It is the initial idea of the whole programme, to develop an experimental setup for the in-situ mechanical characterisation of metal thin films on polymer substrates through bulge testing, where in-situ optical microscopy serves as the characterization instrument.

Crack opening study under optical microscopy is more direct and intuitionistic. In-situ mode gives the opportunity to monitor and record the evolution of cracks visually. Bulge test is an alternative method to apply stress to the membrane, other than micro uniaxial tensile test. We use a spherical window, which provides equi-biaxial tensile stress to the membrane. It is a more powerful simulation of applications of stretchable electronics in spherical form, smart contact lens for example.

After we obtain the control mechanism of the strain using in-situ laser profilometry, we can move to bulge test with in-situ optical microscopy, where the crack opening of gold on PDMS membrane is studied. Crack opening study under optical microscopy is more direct and intuitionistic. In-situ mode gives the opportunity to monitor and record the evolution of cracks visually.

An inverted microscope is used in our experiment, twenty times magnification is the maximum we can achieve. It is enough to observe cracks opening evolution under increasing pressure, i.e. increasing strain of membrane. Crack opening is measured by image processing software imageJ manually, however we believe that the precision and the convenience can be improved in future if an automatic measurement is developed.

6.1 Introduction of Optical Microscopy [31]

Optical Microscopy is well-known by researchers, thus here we just briefly introduce the different classic forms of OM and the type of microscopes, for the consideration that different optical microscopes can cope with bulge test, future researchers may be interested to choose a microscope other than the one we choose. An Inverted Metallurgical Microscope, Olympus IX71 is used in our experiment, equipped with objectives of 4X, 10X and 20X magnification.

1) **Classification by form**

   Optical microscopes can be categorized into two types: upright and inverted, based on the alignment order of specimen, light source and the objective.

   Upright microscopes are with configuration in which the tip of the objective is pointing downward. Observation of the specimen is from above. Light source illuminate the specimen from below.

   Inverted microscopes are with configuration in which the tip of the objective is pointing upward. Observation of the specimen is from below. The objective is underneath the stage. Light can be directed on the specimen from either above or below.

2) **Classification by type of microscopy**

   Bright Field (BF) Microscopy:

   It is the most common optical observation method. It suits the stained and colorful specimens. It can obtain information of the specimen on color and brightness because the entire field of view is brightly illuminated.

   Phase Contrast Microscopy (PC, PH):

   Phase contrast microscopy is suitable for viewing colorless and transparent specimens. Light rays shine to the specimen and refracted while passing

through it. This mechanism brings bright/dark contrast to images. A phase-contrast objective and a condenser is fitted for observation.

Differential Interference Contrast (DIC) Microscopy

Differential interference contrast microscopy is suitable for viewing colorless and transparent specimens. A gradient is used to generate phase difference, and is used to induce bright/dark contrast while the light passes through specimen. The microscope is fitted with a DIC prism and a polarizing plate for DIC observations. DIC can give a 3D observation of specimen by the shadowed appearance of object contours. But some arears are difficult to view maybe due to the orientation of gradients.

Fluorescence (FL) Microscopy

Fluorescence microscopy requires the specimens to be stained with fluorescent dye. A high-intensity ultrahigh-pressure mercury lamp is generally used as light source for generating fluorescence in the specimen. Fluorescence is emitted from a dark field of view, the detectability of this method is relatively high.

Fig.6.1. Inverted Metallurgical Microscope IX71 Olympus

6.2 Setup description

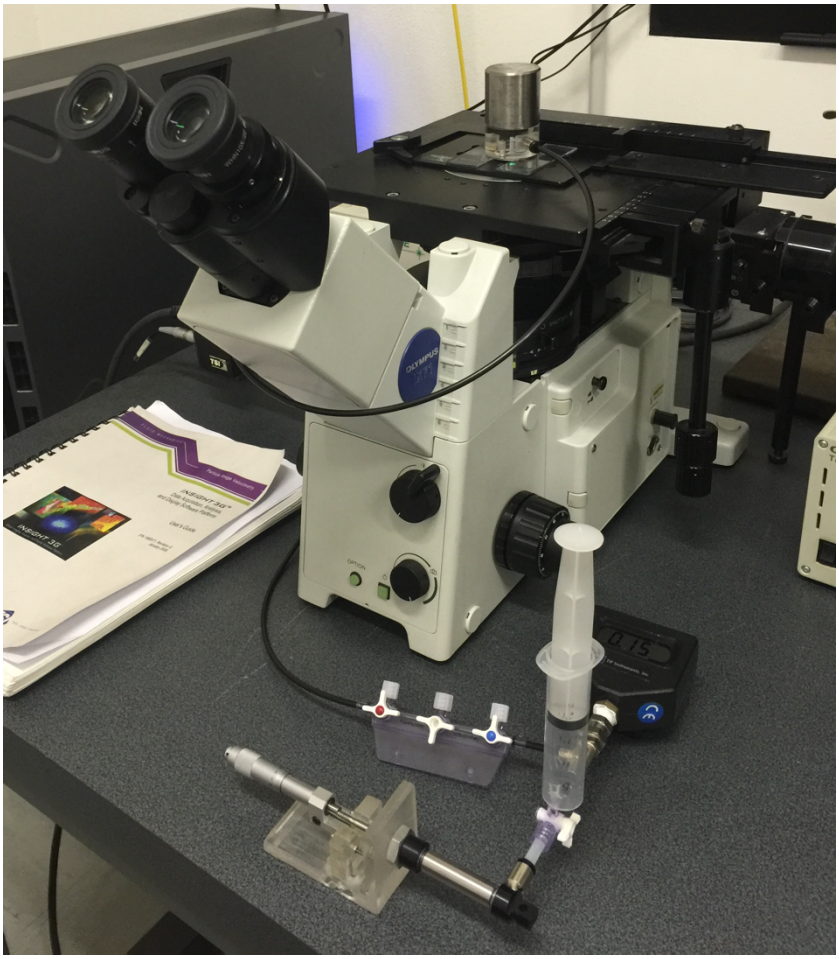

Fig.6.2. Experimental setup for bulge test with in-situ Optical Microscopy

The overall setup is shown in Fig.6.2. There are several key points that need to be mentioned.

Firstly, the bulge device should be firmly fixed on the working stage. Tape is used to stick the device onto the stage. An extra piece of heavy metal is mounted onto the device to keep it firm and unmoved during the experiment. Fixing the position of the device is important, due to the fact that a tiny displacement of it will result in a large shift of image under 20 times magnification. The focused crack may be completely out from view, which will induce difficulties in the data post-processing later.

Secondly, like in the experiment under laser profilometer, the device is also linked to the rest pressure providing and controlling system with a long tube to avoid influence from the manipulation of the microscrewer and the syringe pump. Likewise, the pressure gauge and the microscrewer stage are also stuck on the desk to further reduce the possible vibration during manipulation.

A digital camera is mounted onto the microscopy to record in-situ images of cracks opening under bulge test. The operation software which cope to capture and store images should be open after switching to camera mode. While demounting the setup, light source should be first turned off, the software should then be closed before unplugging power of the camera. The device is demounted from the stage at last.

6.3 Experimental Protocol

The experiment is conducted under the following protocol:

1) Align the bulge test setup as illustrated in Chapter 4.

2) Skip sealing checking step, align the experimental setup as illustrated in 6.2.
   Make sure that the device is firmly fixed on the stage. Though sealing is important for the experiment, checking is still skipped to avoid further induction of new cracks or evolution of pre-existing cracks.

3) Power on camera, switch to camera mode, tune light to sufficient luminance, find out the proper position of the bulge window.
   The position modification is done under four times magnification. An in-situ monitoring is achieved by camera using continuous capturing mode. The spherical window center should be around the center of monitoring screen.

4) Start taking images at zero pressure under each magnification.
   Three different magnification is used. When switching to different objectives, refocusing is necessary to capture image with good quality. One should first use the continuous mode to adjust the focus, and switch to single mode to capture an image. Push ‘stop’ button when a switch between capturing mode is to be made, and repush ‘capture’ once switched, or it may cause error.

5) Increase pressure at interval of 0.05 PSI until it reaches 0.5 PSI, capture images under each magnification.

Different magnifications serve as backup solution of experimental data only, but the sequence we used to study cracks opening evolution is that of 20X magnification.

Refocusing is performed under continuous mode as mentioned before, one should tune the focus in and out several times to find the precise focus. Once the membrane is bulged, one should try to recentralize the image, putting the bulged center as center of the observation view.

A concentric blurring can be seen while tuning the focus in and out. The center of the blurring is the most bulged center of the membrane. One should adjust the stage gently to let the bulged center coincide with the image center. In this manner, the most strained region will be imaged and ready for further study.

Record the sequence and the corresponding pressure.

The reason of taking increment of 0.05 PSI is illustrated in 5.3, the experimental protocol for profilometer. The same reasoning is made here.

6) Increase pressure at interval of 0.1 PSI, until it reaches 1PSI, capture images under each magnification.
The reason to take larger intervals of pressure increment is illustrated also in 5.3.

7) Export images, close the operation software, turn down illumination, unplug camera power, demount the bulge test device.

8) Post processing of data
Details will be illustrated in result section 6.3.

6.4 Results and discussion

The experiment is performed under two different window size, one is 1mm in diameter, the other is 2mm. (SHOW a SEQUENCE OF IMAGES for both)

Different appearance of crack, because of the different window size, same pressure leads to bigger deflection, means, higher strain state.—profilometry before gives p-h, constitutive

Also, the small window images gives a small region of interest which is actually in focus, conversely, a bigger window size, almost all the field of view is in focus, which is suggested that this window size is more suitable for observation addressed. For the 500um window size, the profilometer experimental data is available, it would have been possible to relate the pressure with stress and strain of the membrane by direct comparison with the experimental data. For 1mm window, the deflection range is out of the measurable range of the laser profilometer used. Therefor direct comparision is not possible. But combined with the HBE, we still can predict the p-h behavior, and therefore stress-strain for that window. ininterest
Klsfl;k
Sadf

Final plot: crack opening vs strain/stretch, should coincide for 2 different windows..

7 Conclusion and Recommendations